Multi-model assessment of the deglacial climatic evolution at high southern latitudes

Takashi Obase[1,2], Laurie Menviel[3], Ayako Abe-Ouchi[1], Tristan Vadsaria[1,4*], Ruza Ivanovic[5], Brooke Snoll[5], Sam Sherriff-Tadano[5], Paul J. Valdes[6], Lauren Gregoire[5], Marie-Luise Kapsch[7], Uwe Mikolajewicz[7], Nathaelle Bouttes[8], Didier Roche[8], Fanny Lhardy[8], Chengfei He[9], Bette Otto-Bliesner[10], Zhengyu Liu[11], Wing-Le Chan[1]

[1]Atmosphere and Ocean Research Institute, The University of Tokyo, Kashiwa, Japan

[2]Japan Agency for Marine-Earth Science and Technology, Yokohama, Japan
[3]Climate Change Research Center, The Australian Centre for Excellence in Antarctic Science, the University of New South Wales, Sydney, Australia,
[4]UiT The Arctic University of Norway, Tromsø, Norway
[5]School of Earth & Environment, University of Leeds, Woodhouse Lane, Leeds, UK
[6]School of Geographical Sciences, University of Bristol, University Road, Bristol, UK
[7]Max Planck Institute for Meteorology, Hamburg, Germany
[8]Laboratoire des Sciences du Climat et de l'Environnement/Institut Pierre-Simon Laplace, UMR CEA-CNRS-UVSQ, Université Paris-Saclay, Gif-sur-Yvette, France
[9]Woods Hole Oceanographic Institution, Woods Hole, MA, USA
[10]Climate and Global Dynamics Laboratory, National Center for Atmospheric Research, Boulder, USA
[11]Atmospheric Science Program, Department of Geography, Ohio State University, Columbus, USA
*Now at Biogéosciences, UMR 6282 CNRS, Université Bourgogne Europe, 6 boulevard Gabriel, 21000 Dijon, France

Correspondence to: Takashi Obase (tobase@jamstec.go.jp)

Abstract. The quaternary climate is characterised by glacial-interglacial cycles, with the most recent transition from the last glacial maximum to the present interglacial (the last deglaciation) occurring between ~ 21 and 9 ka. While the deglacial warming at high southern latitudes is mostly in phase with atmospheric CO_2 concentrations, some proxy records have suggested that the onset of the warming occurred before the CO_2 increase. In addition, high southern latitudes exhibit a cooling event in the middle of the deglaciation (15 - 13 ka) known as the "Antarctic Cold Reversal" (ACR). In this study, we analyse transient simulations of the last deglaciation performed by six different climate models as part of the 4th phase of the Paleoclimate Modelling Intercomparison Project (PMIP4) to understand the processes driving high southern latitude surface temperature changes. As the protocol of the last deglaciation sets the choice of freshwater forcing as flexible, the freshwater forcing is different in each model, thus hindering the multi-model comparison. While proxy records from West Antarctica and the Pacific sector

of the Southern Ocean suggest the presence of an early warming before 18 ka, only half the models show a significant warming at this time (~1°C or ~10% of the total deglacial warming). All models simulate a major warming during Heinrich stadial 1 (HS1, 18 - 15 ka) concurrent with the CO_2 increase and with an AMOC weakening in some models. However, the simulated HS1 warming over Antarctica is smaller than the one suggested from ice core data. During the ACR, simulations with an abrupt AMOC increase exhibit a high southern latitude cooling of 1 to 2°C, in relative agreement with proxy records, while simulations with rapid North Atlantic meltwater input exhibit a warming. Using simple models to extract the relative AMOC contribution, we find that all climate models simulate a high southern latitude cooling in response to an AMOC increase with a response timescale of several hundred years, suggesting the choice of the North Atlantic meltwater forcing substantially affects high southern latitudes temperature changes. Thus, further work needs to be carried out to reconcile the deglacial AMOC evolution with the Northern hemisphere ice sheet disintegration and associated meltwater input. Finally, all simulations exhibit only minimal changes in Southern Hemisphere westerlies and Southern Ocean meridional circulation during the last deglaciation. Improved understanding of the processes impacting southern high atmospheric and oceanic circulation changes accounting for deglacial atmospheric CO_2 increase are needed.

1. Introduction

The recent Quaternary climate is characterised by glacial-interglacial cycles of about 100,000-year periodicity (Lisiecki and Raymo, 2005; Jouzel et al., 2007). These glacial-interglacial cycles are driven by insolation changes as external forcing and by feedbacks, including changes in atmospheric greenhouse gas (GHG) concentrations and continental ice sheets (Abe-Ouchi et al., 2013). During the Last Glacial Maximum (LGM, ~21 ka; ka indicates 1000 years before present), the continental ice sheets covered a significant area of the high northern latitudes (Tarasov et al., 2012; Peltier et al., 2015), thus leading to a sea level fall of ~130 meters compared to pre-industrial (Lambeck et al., 2014). The atmospheric CO_2 concentration was also ~100 ppm lower than pre-industrial (Petit et al., 1999; Bereiter et al., 2015). These climatic boundary conditions contributed to a colder climate during the LGM, with global mean surface air temperature anomalies estimated to be 4 to 7 °C lower than present-day (Annan et al., 2022; Liu et al., 2023). As the last deglaciation (transition from the LGM to the early Holocene,

~11 ka) represents one of the largest, most recent and well-documented natural warming of the last million years, an understanding of the processes and feedbacks during this time period can offer insight into our own modern changing world. Here, we focus on the high southern latitudes, where deglacial warming began before their Northern Hemisphere (NH) counterparts (Shakun et al., 2012), and which have been suggested to play a major role in driving the increase in atmospheric CO_2 concentration. Although the timing of the onset of the deglacial warming at high southern latitudes is poorly constrained, a compilation of Antarctic ice core records from East Antarctica suggests that the deglacial Antarctic warming started at ~ 18 ka, in phase with the rise in atmospheric CO_2 concentration (Parrenin et al., 2013). On the other hand, a record from the West Antarctic Ice Sheet Divide ice core (WDC) suggests that the warming started at ~ 20 ka (Shakun et al., 2012; WAIS project members, 2013). Moreover, an early onset of the deglacial warming (~21 ka) at high and mid-southern latitudes has also been suggested based on SST and sea ice records from the Pacific sector of the Southern Ocean (Moy et al., 2019; Sikes et al., 2019; Moros et al., 2021; Crosta et al., 2022; Sadatzki et al., 2023).

Millennial-scale climate events are superimposed on the deglacial warming. At the beginning of the deglaciation, during Heinrich stadial 1 (HS1, ~18 to 14.7 ka, following Ivanovic et al., 2016), Greenland and the North Atlantic region remained cold (Buizert et al., 2014, Martrat et al., 2007), while significant warming occurred at high southern latitudes (WAIS project members, 2010). This period was associated with a weakening of the Atlantic Meridional Ocean Circulation (AMOC), evidenced by Pa/Th in marine sediments (McManus et al., 2004; Ng et al., 2018). During the subsequent Bølling-Allerød (BA, ~14.7 to 12.8 ka) period, Greenland surface air temperatures rose by more than 10°C in just a few decades (Stephensen et al., 2008; Buizert et al., 2014), and the AMOC strengthened significantly (Severinghaus & Brook, 1999; McManus et al., 2004; Roberts et al., 2010; Ng et al., 2018). A cooling event at high southern latitudes, known as the Antarctic Cold Reversal (ACR), was identified between ~15 and 13 ka (Jouzel et al. 2007; Pedro et al., 2016), concurrent with the BA. The Younger-Dryas (YD, 12.8 to 11.7 ka) followed the BA, and was characterised by a drastic cooling in Greenland and the North Atlantic. While the processes leading to the YD are still debated (Renssen et al., 2015), it has been suggested that the YD could be attributed to a weakening of the AMOC (McManus et al., 2004), caused by a rerouting of freshwater into the Arctic that was then transported toward the deep-water formation sites of the

subpolar North Atlantic by coastal boundary currents (Condron and Winsor, 2012; Kapsch et al., 2022). Climate model simulations with marine proxy constraints support the variations in the AMOC during the last deglaciation (Pöppelmeier et al., 2023).

An AMOC weakening causes a warming in the South Atlantic as the meridional oceanic heat transport to the North Atlantic is weakened (Stocker & Johnsen, 2003; Stouffer et al., 2006). This warming can then be propagated to the Southern Ocean and Antarctica (Pedro et al., 2018). The contrasting temperature changes between Greenland and the southern high latitudes can also be found during abrupt events of the last glacial period known as Dansgaard–Oeschger cycles (Dansgaard 1993; NGRIP project members, 2004; WAIS Divide project members, 2015), which have led to the notion of a bipolar seesaw (Stocker and Johnsen 2003; Capron et al., 2010). Alongside these events, the atmospheric CO_2 increase throughout the deglaciation occurred in steps, suggesting a link with millennial-scale climate events (Marcott et al., 2014) and changes in Southern Ocean circulation contributing to degassing of oceanic carbon (Anderson et al., 2009, Menviel et al., 2018).

Transient climate simulations provide a suitable framework for assessing the processes leading to deglacial climate changes. Early transient simulations that were conducted with transient orbital forcing, GHGs and ice sheets suggested that an increase in austral spring insolation in the southern high latitudes was responsible for the onset of warming (Timmermann et al., 2009), and that deglacial warming of the Southern Ocean appeared as early as ~20 to 18 ka in association with sea ice retreat (Roche et al., 2011). Transient simulations that also included freshwater input into the North Atlantic highlighted the AMOC impact on climate change (Liu et al., 2009; He et al., 2011). Menviel et al. (2011) further showed that the ACR could be a response to the strong AMOC increase at the end of HS1, but that its length and amplitude could have been enhanced by meltwater input from the Antarctic ice sheet. These simulations were designed to simulate AMOC changes in agreement with estimates from proxy records, and therefore the magnitude, location, and timing of the implemented meltwater fluxes were idealised. In contrast, experiments forced with meltwater fluxes consistent with ice sheet reconstructions based on sea-level constraints often simulate millennial-scale AMOC changes in disagreement with accepted interpretations of climate and ocean records (Snoll et al., 2024). Some experiments simulate an AMOC weakening at the time of the BA because of significant mass loss of NH ice sheets (Bethke et al., 2012; Ivanovic et al.,

2018a; Kapsch et al., 2022; Bouttes et al., 2023) or do not simulate any abrupt climate events (Gregoire et al., 2012). With an idealised scenario that follows the evolution of NH ice sheets more closely (except for the 14 ka meltwater pulse), the MIROC climate model shows that it is possible to simulate an abrupt AMOC strengthening with the presence of continuous freshwater in the North Atlantic because of gradual warming (Obase and Abe-Ouchi, 2019). These studies indicate that different models have different sensitivities in terms of the AMOC response to forcing and, therefore, it is useful to analyse multi-model results for a robust understanding of the climatic processes.

To facilitate further examination of the mechanisms driving deglacial climate change, a protocol for carrying out transient simulations of the last deglaciation was proposed as part of the fourth phase of the Paleoclimate Modeling Intercomparison Project (PMIP4) (Ivanovic et al., 2016). The protocol of PMIP4 deglaciation summarised climate forcings needed (ice core based atmospheric GHGs and reconstructed ice sheets) for climate model experiments. The protocol is designed to be flexible in that the use of some boundary conditions is determined by each modelling group, which allows an exploration of different climate scenarios. The first PMIP multi-model study of the last deglaciation, focusing on the northern hemispheric climate during HS1, found that different freshwater approaches (*melt-uniform*, *melt-routed*, *trace-like*, *bespoke*, Snoll et al. (2024)) have a dominant impact on North Atlantic climate variability. While this finding could be drawn due to the flexibility of the PMIP deglaciation protocol (Ivanovic et al., 2016) regarding the choice of the method on how to distribute the freshwater forcing, this flexibility makes it challenging to properly compare the simulations. Nevertheless, the multi-model assessment of the last deglaciation performed here provides an opportunity to investigate the processes impacting southern high latitude climate and to evaluate the uncertainties from the models' sensitivity to the forcings.

Some boundary conditions for climate models, including GHG and Antarctic ice sheet (prescribed in PMIP4 protocol), result from climate change at high southern latitudes. Proxy records (Sigman et al., 2010, Skinner et al., 2010, Martinez-Garcia et al., 2011) and modelling studies (Bouttes et al., 2012, Menviel et al., 2016, Menviel et al., 2018, Gottschalk et al., 2019) indicate that physical and biogeochemical changes in the Southern Ocean may have significantly contributed to ocean carbon uptake during the last glacial period and to the atmospheric CO_2 increase during HS1. Subsurface warming on

the Antarctic shelf contributes to the mass loss of Antarctic ice sheets through enhanced melting of ice shelves, and retreat of grounding lines (Golledge et al., 2014; Lowry et al., 2019). In addition, climate conditions at high southern latitudes can impact the formation of Antarctic Bottom Water (AABW) and the shoaling of AMOC (Sherriff-Tadano et al., 2023). Hence investigating the deglacial climate evolution at high southern latitudes may give an insight into critical climate system feedbacks.

Here, we analyse the deglacial climatic evolution (21–11 ka) at high southern latitudes as simulated in six PMIP4 transient experiments, and compare the results with paleo-proxy records. We focus on the magnitude and rate of changes in Antarctic surface air temperature (SAT) and Southern Ocean sea surface temperature (SST). As there is a substantial difference between the temporal evolution of AMOC strength in the simulations, we utilise statistical or simple models to separate the impact of changes in atmospheric CO_2 and AMOC on Southern Ocean SST. Finally, we analyse the evolution of the AABW, Southern Ocean westerlies and subsurface ocean temperature in the Southern Ocean to discuss critical climate system feedbacks occurring at high southern latitudes.

2 Methods

2-1 Climate models and experiments used in this study

We use the PMIP4 transient simulations of the last deglaciation performed with six atmosphere-ocean coupled climate models (Table 1), and analyse the time period from the LGM to the Early Holocene 21–11 ka. Table 2 summarises the experimental design of each model simulation and their reference articles, with the evaluation of their LGM and PI states mentioned in their description. The LGM climate fields (initial condition of these experiments) have been evaluated by previous studies, particularly for global temperature changes (Kageyama et al. 2021), sea ice and SST changes in the Southern Ocean (Lhardy et al., 2021; Green et al. 2022), and SAT changes over the Antarctic ice sheet (Buizert et al. 2021). A part of the transient simulations utilized in this study have also been compared to proxy-reconstructions (Weitzel et al. 2024). Fig. S1 compares simulated sea-ice edges for the pre-industrial simulations from six models used in this study, which shows some models underestimate pre-industrial summer sea ice extent, but mostly to an acceptable level. The Equilibrium Climate Sensitivity (ECS, defined by global mean SAT changes in response to doubling CO_2 from the pre-industrial) of each model

ranges from 2.0 to 3.9 ℃, and the global mean surface air temperature (SAT) anomaly for the LGM is 3.5 to 7.3 ℃ (Table 1). While some of the modelling groups performed two or more sensitivity experiments with different model parameters or boundary conditions (e.g., different freshwater forcing (FWF) scenarios or ice sheets), for this study we have selected one representative simulation from each climate model. Fig. 1 summarises the time evolution of the climate forcings, i.e. insolation, atmospheric GHGs, and continental ice sheets used in the simulations. Both reconstructions (ICE-6G_C VM5a, henceforth 'ICE-6G_C'; and 'GLAC-1D') have larger Antarctic ice sheet volume at the LGM, with a ~ 10 m sea-level equivalent volume change at the LGM, relative to present-day. Both suggest ~ 100 m of elevation reduction since the LGM at EPICA Dome C (EDC, 123°E, 75°S), while WAIS Divide (WDC, 112°W, 79.5°S) differs by 300 m between the two datasets (Fig. 1d).

Fig. 2a summarises the total amount of FWF in the NH in six simulations. The FWF schemes can be classified into two groups: The first group with FWF adjusted to reproduce large-scale AMOC variability (iTRACE, LOVECLIM, MIROC), and the second group with FWF consistent with the reconstructed ice volume changes (HadCM3, MPI-ESM, iLOVECLIM) based on ICE-6G_C or GLAC-1D (Fig. 2a, upper panel, red and black lines). Notably, during HS1, iTRACE and LOVECLIM have significant FWF (~ 0.2 Sv), while other simulations apply FWF of less than 0.1 Sv. In LOVECLIM and MIROC, the meltwater flux was uniformly applied to the North Atlantic, while other models use the location of the melting NH ice-sheet and associated runoff to apply a spatially varying FWF (Table 2). ICE-6G_C (HadCM3, MPI-ESM, iLOVECLIM) leads to a meltwater input of about 0.1 Sv to the Southern Ocean at 11.5–11 ka. iTRACE and LOVECLIM also applied freshwater flux to the Southern Ocean to simulate the ACR (iTRACE: up to 0.2Sv during 14.4–13.9 ka, LOVECLIM: fixed at 0.09Sv during 14.67–14.1 ka).

In section 3.3, we conduct further analysis to examine the processes driving Southern Ocean SST using a multilinear regression (MLR) model and a thermal bipolar seesaw model adapted from Stocker and Johnsen (2003).

2-2: Simple models to disentangle CO_2 and AMOC

2-2-1: Multilinear Regression model

We use a MLR model to regress changes in SST onto CO_2 and AMOC variations:

$$SST = \alpha_1 * CO_2 + \beta_1 * AMOC + \gamma \quad , (1)$$

where *SST*, and *AMOC* (defined as the maximum meridional overturning streamfunction in the North Atlantic, at depths below 500 m and 20–60°N) are output from the climate models, and CO_2 is the forcing used in each simulation. γ is the intercept. The AMOC in the analysis is normalised with respect to the temporal maximum and minimum values in each model. The CO_2 is also normalised with respect to the total change between 21 and 11 ka (~83 ppm). The MLR analysis is applied to the 2-D fields of the Southern Ocean SST. The same analysis is applied to the Southern Ocean SST averaged over 55–40°S. To focus on long-term climate change and reduce interannual variability, every 100-years, mean SST, AMOC, and CO_2 from 20 to 11 ka are used as the input for this analysis, so each dataset has 90 time-slices. While we use CO_2 as a representation of a gradual forcing as the input of the MLR model, we note that other forcing, such as from ice sheets and orbital changes can contribute to the warming. On the other hand, sensitivity experiments evaluating the contribution of each forcing show that they have a minor impact on Southern Ocean SST and Antarctic SAT changes between 19 and 15 ka (He et al. 2013). The results with coefficient of determination are displayed in Table 3.

2-2-2: Thermal bipolar seesaw model

As the MLR model does not consider transient climate response, we construct a thermal bipolar seesaw model following Stocker and Johnsen (2003). The original thermal bipolar seesaw model is based on an energy balance between the North and South Atlantic Oceans. We add the effect of CO_2 on temperature, which was not considered in the original model. The thermal bipolar seesaw model in this study solves the temporal evolution of Southern Ocean SST using the following equations:

$$\frac{d\Delta SST}{dt} = \frac{\Delta SSTeq - \Delta SST(t)}{\tau} \quad (2)$$

$$\Delta SSTeq = \alpha_2 * CO_2(t) + \beta_2 * AMOCm(t) \quad (3)$$

where $\Delta SSTeq$ is an equilibrium Southern Ocean SST (change since the LGM) expected from the CO_2 and state of the AMOC at time *t*. $\Delta SST(t)$ is the SST change since LGM at time *t*, and τ is the characteristic timescale of the bipolar seesaw. $CO_2(t)$ is the CO_2 concentration at time *t*, and is normalised with maximum and minimum values as in the MLR model. The term *AMOCm(t)* represents the modes of the AMOC from the climate model outputs. When using the simulated AMOC within the bipolar seesaw

model, it is assumed that the AMOC modes are binary, unlike the continuous values in the model. Based on Figure 2, we assume that the AMOC is in a strong mode ($AMOCm(t)$=0) if the AMOC is greater than 14 Sv.

At first, we conduct systematic sensitivity experiments to calculate the minimum root mean square error between the actual ΔSST and the bipolar seesaw model. We conduct 9610 sensitivity experiments for each model within the parameter ranges shown in Table 4. The combination of parameters that gives the minimum root mean square error, along with coefficient of determination between the climate models' SST changes and bipolar seesaw models are displayed in Table 5.

3. Results

3-1: AMOC

As AMOC variations can impact southern high latitude climate, we summarise here the transient evolution of the AMOC in the different simulations. As detailed below, the AMOC evolution is substantially affected by the FWF schemes. All simulations except for MIROC display a strong (~20 Sv) AMOC at the LGM (Fig. 2b), while MPI-ESM and iLOVECLIM shows slightly weaker LGM AMOC in their sensitivity studies where GLAC-1D ice sheet was used (Kapsch et al., 2022; Bouttes et al., 2023). The more vigorous LGM AMOC compared to Pre-Industrial (PI) is in line with the majority of PMIP4 simulations (Kageyama et al., 2021), although it is not consistent with LGM reconstructions from multiple marine tracers (Lynch-Stieglitz et al., 2007; Bohm et al., 2015, Menviel et al., 2016). During the period corresponding to HS1, the AMOC stays weak in MIROC and substantially declines in the iTRACE and LOVECLIM simulations, as meltwater is added into the North Atlantic. On the other hand, in the other simulations, there is only a slight reduction in AMOC (~1 Sv) as the meltwater input into the North Atlantic stays below 0.05 Sv. At the BA (~14.7 ka), three models exhibit an abrupt change from weak to strong AMOC, triggered by a rapid reduction in FWF (iTRACE and LOVECLIM) or as a response to the gradual background warming (MIROC). These simulations, featuring an AMOC strengthening, broadly agree with marine proxy records (Fig. 2b black line). On the other hand, the other three simulations (HadCM3, MPI-ESM, iLOVECLIM) display an AMOC weakening due to a substantial increase in FWF originating from the ice sheet collapse associated with Meltwater Pulse 1a (Deschamps et al., 2012).

During the Younger-Dryas (12.8–11.7 ka), iTRACE, LOVECLIM, and MIROC simulate a weakened AMOC state compared to BA, corresponding to an increase in FWF or an oscillatory nature of the AMOC in MIROC (Kuniyoshi et al., 2022). HadCM3 simulates a small but gradual AMOC reduction throughout the YD, while MPI-ESM exhibits multi-centennial AMOC variability. At 11 ka, the AMOC strength returns to a strong mode except for iLOVECLIM, which stays weak after the BA.

3-2-1: 21–18 ka (onset of warming) and 18–14.7 ka (HS1)

Fig. 3 summarises the simulated Antarctic SAT (Fig. 3c-d) and Southern Ocean SST (Fig. 3e) changes since the LGM in all the simulations (LGM is defined as 21 ka in most models, with some exceptions because of different initialisation; 20.0 ka for iTRACE, 20.6 ka for LOVECLIM). The SAT at WDC and EDC are compared with the ice core based reconstructions from Parrenin et al. (2013) and Buizert et al., (2021). Three models (MIROC, HadCM3, MPI-ESM) exhibit a gradual ~1℃ warming between 21 and 18 ka at both WDC and EDC (Fig. 3c). This simulated EDC warming is comparable with ice core estimates, with MPI-ESM overestimating the warming at the EDC site (Fig. 4a). However, the magnitude of warming suggested from WDC (~2℃ warming between 19.5–19 ka, Shakun et al., 2012) is not fully simulated by any of the models, with iTRACE exhibiting slight cooling (Fig. 4a). MIROC, HadCM3 and MPI-ESM simulate a SAT increase over Antarctica and a 0.5–1.0℃ SST increase in the Southern Ocean north of the sea ice edge, with a gradual reduction in Southern Ocean sea ice area (Figs. 3f and 4b).

All models exhibit a larger warming between 18 and 14.7 ka (i.e. HS1) than between 21 and 18 ka. iTRACE simulates the largest warming in SAT at WDC and EDC (+6–8℃, Figs. 3c-d), closely following the estimates from ice core data. The sharp increase in temperature in iTRACE starts at ~18 ka, corresponding to a period of major reduction in AMOC strength (Fig. 3b). The warming in MPI-ESM follows iTRACE with a 5℃ warming, despite a minor reduction in AMOC strength. The HadCM3 exhibits ~4℃ warming at WDC and ~2℃ warming at EDC, while the other models simulate a 2–4℃ warming at EDC and WDC (Fig. 3c–d). iTRACE exhibits Southern Ocean SST increase of 5 ℃ and LOVECLIM exhibits a sharp Southern Ocean SST increase of ~3℃, in response to an AMOC reduction at ~17 ka. The other models' Southern Ocean SST increase by 1–2 ℃ (Fig. 3e). Southern Ocean sea ice

area exhibits the same trends as the Southern Ocean SST, with iTRACE simulating the largest sea ice area reduction of up to 40% compared to the LGM (Figs. 3f). Noting that iTRACE has the largest LGM sea ice extent (Fig. 4b).

3-2-2: 14.7–13 ka (BA) and 13–11 ka (YD and Holocene onset)

Three models (iTRACE, LOVECLIM, MIROC) simulate an abrupt AMOC increase at the BA onset (Fig. 3b), and a concomitant cooling at high southern latitudes: ~1-2 ℃ Antarctic SAT and Southern Ocean SST decrease (Fig. 3c-e). iTRACE and LOVECLIM exhibit a sharp cooling in Southern Ocean SST and SAT in the early phase of the BA (Fig. 3e), probably enhanced by the meltwater flux into the Southern Ocean (Menviel et al., 2011). In contrast, the three other models (HadCM3, MPI-ESM, iLOVECLIM) exhibit a warming in the early phase of the BA, corresponding to an AMOC weakening. Subsequently, HadCM3 and MPI-ESM exhibit a gradual cooling over the Antarctic and Southern Ocean as the AMOC strengthens in the later part of the BA (~13.5 ka). iLOVECLIM displays a rapid warming at 13.5 ka, followed by a cooling, which is explained by abrupt surface albedo changes caused by the evolving land-sea mask in the Antarctic region (Bouttes et al., 2023).

During YD (13–11ka), iTRACE, LOVECLIM, and MIROC simulate an AMOC weakening as well as a high southern latitude warming. iTRACE simulates a ~3–4℃ increase in Southern Ocean SST, while LOVECLIM and MIROC simulate a 1℃ warming. MPI-ESM exhibits multi-centennial variability associated with variations in AMOC strength. MPI-ESM and iLOVECLIM exhibit sharp cooling in Southern Ocean SST and SAT starting at ~11.5 ka, enhanced by the meltwater flux into the Southern Ocean (Kapsch et al., 2022).

The proxy-record based estimates on total deglacial (21–11 ka) warming is 10 ℃ in WDC, while the EDC estimates range from 5 to 10 ℃ (Parrenin et al., 2013; Buizert et al., 2021). Across the simulations, a 2 to 10 ℃ warming is simulated over Antarctica (Fig. 3c-d). In line with the WDC and the upper range of EDC estimates, iTRACE and MPI-ESM display a 8–10 ℃ total warming over Antarctica. Since the LGM, the Southern Ocean sea ice edge retreats poleward by 10° latitude in models with the largest sea ice retreat (Fig. 5). A SST increase of up to 6 ℃ is simulated in the Southern Ocean near the winter sea ice edge in iTRACE, LOVECLIM, HadCM3, and MPI-ESM, while a ~4 ℃ SST increase is simulated in MIROC and iLOVECLIM (Fig. 5).

The different magnitudes of warming during HS1 and YD between models could be explained by the range of temperature changes between LGM and PI, as the mean SAT and SST changes are different by a factor of two (Table 1). To reduce this model difference, Antarctic SAT are normalised by the temperature anomaly between LGM and PI in Figure 6. When normalised, the simulations with a weak AMOC during HS1 show the largest warming over Antarctica (Fig. 6 left). The normalised Antarctic SAT change at 11 ka lies in between 0.6 and 0.8 with respect to the total temperature change between LGM and PI for five out of six models, indicating additional warming is simulated between 11 and 0 ka in the model simulations. This is different from ice core reconstructions, in that the temperature at 11 ka is comparable to the pre-industrial values (Parrenin et al., 2013; Buizert et al., 2021).

3-3: SST – CO_2 – AMOC relationship analysis

The simulated AMOC time series display large differences across simulations due to different FWF groups, which complicates the quantification of CO_2 forcing and AMOC changes in driving high southern latitude temperature changes in each model. To overcome this, we examine the Southern Ocean SST trajectory against CO_2 forcing, and AMOC strength (Fig. 7). Fig. 7 shows that the deglacial increase in atmospheric CO_2 has major impacts on the Southern Ocean SST because the temperature trajectory is mostly proportional to CO_2 changes unless there are major AMOC changes. Temperature changes associated with changes in AMOC are superimposed on Southern Ocean SSTs, in that a weaker AMOC compared to the long-term mean of respective models (blue circles) tends to induce a warming, and vice versa. Even though the actual time series of AMOC in each model are very different, this result suggests that high southern latitude temperature changes can be decomposed into the effects of CO_2 and AMOC. The relative importance of CO_2 and AMOC are quantified in the following subsections.

3-4: Results of MLR and bipolar seesaw model

The results of the MLR model indicate that the CO_2 coefficients range from 1.0 to 6.5℃ for the total deglacial CO_2 changes (Table 3). All models have a negative coefficient of AMOC (–0.3 to –2.4℃), indicating a Southern Ocean SST increase associated with an AMOC weakening. The regression against Southern Ocean 2-D SST fields indicates that the CO_2 coefficient is mostly positive over the Southern Ocean, ranging from ~0.5 ℃ in the Antarctic zone where sea ice is present until 11 ka, to 2–6 ℃ in the

Southern Ocean north of the LGM winter sea ice edge (Fig. 8). The sensitivity to the AMOC is mostly negative in the Southern Ocean, and areas of high sensitivity overlap with those of CO_2, suggesting sea ice modulates the areas sensitive to both CO_2 and AMOC changes.

Table 5 summarises the results of the bipolar seesaw model. All models have positive CO_2 coefficients (2.0–6.0°C) and negative AMOC coefficients (–0.5 to –2.9°C), as in the MLR models. The time series simulated by the bipolar seesaw model are compared with actual SST changes and with MLR models in Fig. 9. The bipolar seesaw model succeeds in reproducing a gradual SST decrease as a result of an AMOC strengthening (e.g. gradual cooling in iTRACE and MIROC, 15–13 ka). This gradual cooling was not represented by the MLR model, which exhibits an immediate SST response to AMOC changes. The response time ranges from 100–700 years, with most models ranging from 500–700 years with the exception of LOVECLIM and iLOVECLIM (Table 5). We also applied the bipolar seesaw model by using AMOC and CO_2 coefficients from six different models (Table 5), but common inputs of CO_2 (Bereiter et al., 2015) and AMOC from iTRACE. The results indicate that all models would have simulated a cooling at the surface of the Southern Ocean during BA if there was an increase in the AMOC at the beginning of BA as simulated in iTRACE, LOVECLIM or MIROC (Fig. S2).

We note that the values of the CO_2 sensitivity from the MLR and bipolar seesaw model may include gradual forcing from other greenhouse gases, ice sheets, and orbital forcing. In addition, a sharp cooling associated with freshwater in the Antarctic Ocean was not represented because both models, MLR and bipolar seesaw, do not consider meltwater in the Southern hemisphere (~14.5 ka of iTRACE and LOVECLIM, ~11.5 ka of MPI-ESM and iLOVECLIM)

3-5: Other Southern Ocean climate variables

We further analyse AABW transport (minimum global meridional overturning streamfunction, at depths below 3000 m and 60°S–30°S) as an indicator of Southern Ocean meridional circulation, and 850 hPa zonal mean winds over the Southern Ocean (zonal mean winds averaged over 65°S–40°S), to discuss potential impact on deglacial CO_2 changes, which is prescribed in the experiments. We focus on the onset of deglaciation (21–18 ka) and the initial significant increase in CO_2 (~HS1, 18–15 ka). The AABW (Fig. 10b) at the LGM ranges from 10 to 30 Sv among the six models and stays relatively constant between 21

and 18 ka. In the subsequent period (18–15 ka), iTRACE exhibits a gradual decline in the AABW, in phase with Southern Ocean SST changes (Fig. 10d). LOVECLIM and MPI-ESM exhibit a gradual decline in AABW (~5 Sv), while three other models (MIROC, HadCM3, iLOVECLIM) exhibit a small reduction or a stable AABW. Thus, while all models simulate Southern Ocean SST warming and sea ice retreat during HS1, the trends in AABW differ. In addition, the AABW changes do not depend on the AMOC evolution and thus FWF groups (Fig 10a–b). The zonal winds over the Southern Ocean exhibit slight change between 21 and 18 ka, apart in MIROC and MPI-ESM, which exhibit a slight weakening (Fig. 10c). Between 18 and 15 ka, the zonal winds continue to decline in MIROC and MPI-ESM, and start to decline in iTRACE and LOVECLIM. Little changes in zonal winds are simulated in iLOVECLIM, while HadCM3 exhibits a ~10% strengthening.

Subsurface ocean temperatures south of 60°S at depths of around 500 m (Fig. 10e) exhibit an increase during HS1 in 4 of the 6 simulations, with the largest warming (1.2 °C and 0.8 °C) simulated by the two simulations which exhibited the largest SST increase (iTRACE and MPI-ESM). During the BA (15–13 ka), iTRACE and MIROC exhibit a gradual sub-surface temperature decrease while HadCM3 and MPI-ESM exhibit a continuous warming, as per the SST changes in the respective models. iLOVECLIM and LOVECLIM exhibit small changes (<0.5°C) in the total sub-surface temperature. Abrupt subsurface warming in iTRACE (~14 ka) and LOVECLIM (14.8–14.2 ka) coincide with Southern Ocean SST reduction, suggesting that this results from enhanced Southern Ocean stratification as a response to Southern Ocean meltwater input (Menviel et al., 2011; Lowry et al., 2018).

3-6: Additional freshwater experiments on HS1 SO warming in MIROC and HadCM3

We additionally show two simulations run with the MIROC and HadCM3 models to assess the impact of FWF on southern high latitude climate during HS1. We remind that the MIROC and HadCM3 comes from different freshwater groups (Fig. 2). In the MIROC simulations, the FWF during HS1 is increased to 0.1 Sv or 0.2 Sv between 18 and 15.5 ka (Figure 11a, red and orange lines) instead of 0.03 Sv in the standard simulation. This larger meltwater input further weakens the AMOC (Fig. 11a) and leads to an additional 1 ℃ SST increase in the SO compared to the standard simulation (Fig. 11d). The 1 ℃ warming in response to AMOC reduction of ~5 Sv is higher than results from the MLR and bipolar seesaw models. In the HadCM3 simulations, a North Atlantic freshwater flux of ~0.2 Sv during HS1

(similar to Trace-21ka A, Liu et al., 2009) reduces the AMOC by 15 Sv (Fig. 11e blue lines), and induces an additional ~1 ℃ increase in Southern Ocean SST compared to the standard simulation (Fig. 11h). The simulated HS1 warming in HadCM3 is consistent with both MLR and bipolar seesaw models (Tables 3 and 5). The results from the MIROC and HadCM3 sensitivity experiments show that the simulated warming during HS1 can be twice as strong with an AMOC shutdown compared to the standard simulation of each model. As in the LOVECLIM Heinrich stadial 4 simulation (Figure S2; Margari et al. 2020) the warming in the southern high latitude in response to AMOC strength is not necessarily linear, while MLR models assume a linear temperature response to the AMOC.

4. Discussion

4-1: Onset of deglacial warming

The climate forcing in the early deglaciation primarily comes from insolation due to obliquity and precession changes (Fig. 1a), which leads to an increase in spring to summer insolation south of 60 °S (Fig. S3). Ice core data suggest that the onset of deglacial warming at WDC was earlier than the increase in CO_2, and this early deglacial warming has been suggested to result from an AMOC reduction (Shakun et al., 2012) or local insolation changes (WAIS project members, 2013). However, simulated early warming is smaller than proxy records. Three models (MIROC, HadCM3, MPI-ESM) exhibit a small but warming (~ 0.5℃) between 21 and 18 ka (Fig. 4a) in both West and East Antarctica, as well as at the surface of the Southern Ocean, primarily in the Pacific sector (Fig. 4b) as suggested by proxy records (Moy et al., 2019; Sikes et al., 2019; Moros et al., 2021). The amplitude of the early warming in these models is comparable to a previous modelling study (Timmermann et al., 2009), while the other models show a slight cooling (iTRACE) or little change (LOVECLIM and iLOVECLIM).

The first explanation for the differences in the simulated temperature change between 21 and 18 ka is the Southern Ocean sea ice at LGM. MIROC, HadCM3 and MPI-ESM have less LGM summer sea ice than other models. The smaller sea ice extent at the LGM, relative to other models, may lead to a high sensitivity to increased insolation during austral spring to summer, causing significant warming with sea ice retreat (Timmermann et al., 2009; Roche et al., 2011). If the LGM Southern Ocean sea ice extent is extensive, the increase in insolation primarily south of 60 °S (Fig. S3) does not warm the Southern Ocean

as much because of high sea ice albedo. Although the local insolation changes are the likely cause of an early warming simulated in some of the models, the addition of freshwater could contribute to the AMOC weakening. For example, the consideration of an additional freshwater flux from the Fennoscandian ice sheet in the freshwater forcing prior to 18 ka as included in MPI and as suggested by Toucanne et al. (2010), would weaken the AMOC and lead to a more pronounced warming in the southern high latitudes.

Another model-data difference is the different early warming rates between West and East Antarctica. The data from WDC suggest there was significant warming in West Antarctica, while a less significant change in East Antarctica is suggested by EDC. In contrast, the models simulate similar warming rates in both West and East Antarctica (Fig. 4a), suggesting the models may underestimate the spatial heterogeneity in West and East Antarctic warming. This might be attributed to the Antarctic ice sheet history prescribed in the experiments, where both ICE-6G_C and GLAC-1D have minor surface elevation changes at WDC in the early deglaciation (Fig. 1d). Buizert et al. (2021) used the MIROC and HadCM3 models and showed that the uncertainty in Antarctic ice sheet height affects the difference between LGM and PI temperatures because changes in surface elevation affect SAT (~1 °C warming per 100 m altitude reduction). This might suggest that the lower surface elevations at WDC, related to the ice sheet terminus retreat between 20–15 ka in the Amundsen Sea (Bentley et al. 2014), may have contributed to the early deglacial warming primarily in West Antarctica. The coarse resolution of the atmospheric models (2.5 to 5.6 degrees in the horizontal) may impact the warming contrast between East Antarctica (EDC ice core site) and West Antarctica (WDC ice core site) through an inherent smoothing of the surface topography of the Antarctic ice sheet and the associated impact on the atmospheric circulation (Buizert et al., 2021). In addition, the relatively coarse resolution of the ocean models (1 to 3 degrees), may impact the AMOC sensitivity to iceberg and freshwater flux in the North Atlantic (Condron and Winsor 2012), or the impact of mesoscale processes in the Southern Ocean (Morrison et al., 2013) and their response to the deglaciation.

Uncertainty in the Antarctic ice sheet topography could also explain some model-data differences during the early Holocene, where simulations indicate that an additional warming occurs after 11 ka (Fig. 6). This is different from ice core data (Fig. 4) and global mean ocean temperature (including deep-sea temperature) estimated from noble gases in ice cores, which suggests that temperatures reach Holocene

levels at the end of YD (Bereiter et al., 2018). The decrease in surface elevation of the Antarctic ice sheet after 11 ka (Fig. 1e) may contribute to the Holocene warming. It would be valuable to assess the uncertainties from ice sheet reconstructions, as new reconstructions have been published (e.g., Gowan et al., 2021), and different LGM ice sheets can induce different AMOC variabilities (Prange et al., 2023; Masoum et al., 2024).

4-2: Rate of temperature changes

HS1 (~18–14.7 ka) exhibits major warming in all models because of the CO_2 increase, with the total warming being dependent on the sensitivity of each model to CO_2, and to AMOC changes. In turn, the deglacial AMOC evolution is dictated by the glacial meltwater input, as shown in additional sensitivity experiments performed with MIROC and HadCM3 (Fig. 11). iTRACE simulates the largest warming during HS1 among six models, with an Antarctic SAT increase of 6–8℃ and Southern Ocean SST of 4–5℃. While the Antarctic SAT matches ice-core data, Southern Ocean SST is larger than the SST stack. Five models besides iTRACE simulate a Southern Ocean SST change which compare well with the SST stack data, but these five models underestimate Antarctic SAT. This indicates that the different magnitudes of warming between Southern Ocean SST and Antarctic SAT are not fully represented in models. While iTRACE exhibits the largest cooling of global mean SAT at the LGM compared to PI (7.3 ℃, compared to the six-model mean of 5.3 ℃), the ECS of iTRACE (3.6 ℃) is not the highest among the six models; instead, MIROC4m has the highest ECS despite weaker deglacial warming (Table 1). We examine the relationship between ECS and the LGM global mean SAT changes using multi-model PMIP3 and PMIP4 simulations (Fig. S4). We find a weak negative correlation (–0.06) between the ECS and global mean LGM SAT changes, and the local SAT change in the individual climate models can vary by about a factor of two even with the same ECS. A substantial asymmetry between warm and cold climates has been identified in previous studies because of the presence of continental ice sheets, ocean dynamics, and cloud feedback (Yoshimori et al., 2009; Zhu and Poulsen, 2021). Hence, understanding the mechanism and amplitude of cooling in the LGM simulations will contribute to a better understanding of multi-model differences in the deglacial warming.

The sensitivity to AMOC ranges between (–0.5 to –2.9℃) based on the analysis using the thermal bipolar seesaw model (Table 5). A multi-model study comparing freshwater hosing experiments of 11

climate models (including LOVECLIM, MIROC, and HadCM3 used in this study) under LGM climate shows that most models exhibit warming in the Southern Ocean (Kageyama et al., 2013). However, the simulation length in their study is less than 420 years. In this study, we estimated the timescale for the bipolar seesaw to be ~500–700 years. Thus, longer simulations are needed to evaluate the extent of the climate response at high southern latitudes.

The MLR and thermal bipolar seesaw models in this study include several assumptions. Firstly, as the gradual forcing is represented only by the CO_2 concentration, they do not consider the effect from retreating ice sheets, meltwater flux in the Southern Ocean, or insolation changes explicitly. Other forcings could be included in the CO_2 or AMOC coefficients in this analysis. For instance, insolation change in Northern summer have positive correlations with the CO_2 because both exhibit gradual increase (Fig. 1a-b). Antarctic and Northern Hemisphere ice sheet changes could impact Southern Ocean SST (Abe-Ouchi et al., 2015). This may explain the CO_2 coefficients from the MLR and bipolar seesaw model that are higher than expected from the ECS value. On the other hand, the AMOC sensitivity of the LOVECLIM model is low compared to the 1.5 ℃ Southern Ocean SST increase found in the simulation of Heinrich stadial 4 (Margari et al. 2020, Fig. S5), and the CO_2 coefficient is quite high, potentially implying a poor separation of the two factors.

4-3: Freshwater forcing and temperature changes in southern high latitudes

As shown here, the deglacial AMOC variations are quite different amongst the simulations. Only those which display an AMOC increase at the end of HS1 can capture a cooling trend at BA (corresponding to the ACR) as suggested by ice-core data (iTRACE, LOVECLIM, MIROC). In comparison to previous transient simulations of the last deglaciation, the representation of the duration of the ACR has improved, as it was previously simulated as too short (Lowry et al., 2018). On the other hand, individual climate model simulations that are forced with a large NH meltwater pulse consistent with ice sheet reconstructions do not simulate an increase in the AMOC at the BA (Ivanovic et al., 2016; 2018; Kapsch et al., 2022; Bouttes et al., 2023). FWF in the NH and associated reduction in the AMOC lead to Antarctic warming during HS1 in the sensitivity experiments with individual forcing (He et al., 2013) and sensitivity experiments with FWF (Figure 11). A comparison of the six models reveals that capturing phase changes in the AMOC is necessary to simulate warming or cooling trends at southern

high latitudes. This is also supported by results of the bipolar seesaw models forced with a common AMOC (Fig. S2). While MIROC simulates a rapid increase in the AMOC at BA transition with a continuous freshwater flux (Fig. 2), a greater FWF by a factor of 1.5 leads to a weak AMOC throughout the last deglaciation (Obase et al., 2021). Thus, the simulated temperature changes at southern high latitudes are sensitive to FWF in the NH. However, the timing and magnitude of meltwater input inferred from ice sheet reconstructions is still different from meltwater needed to obtain a deglacial climate evolution in agreement with proxy records. This so-called meltwater paradox (Ivanovic et al., 2018; Snoll et al., 2024) is present for a major periods of the last deglaciation including the BA transition and HS1, suggesting a need for a better assessment of freshwater scenarios, and a need to assess the sensitivity of climate models to freshwater forcing, and the necessity to reduce potential climate model biases. We also note that the routing location of meltwater input (Roche et al., 2010; He et al., 2020) and the consideration of icebergs and meltwater discharge into the ocean (Schloesser et al., 2019; Love et al., 2021) may induce different AMOC changes. In addition, FWF from the Antarctic ice sheet can enhance the ACR, as found in iTRACE (~14.2 ka) and LOVECLIM (~14.7 ka), with a sharp cooling in Southern Ocean SST and Antarctic SAT primarily in WDC. This is caused by the intensified stratification in the Southern Ocean (Menviel et al., 2010; 2011), which induces significant warming in the subsurface and contributes to further mass loss from Antarctic ice sheets (Golledge et al., 2014). As ice core data does not exhibit such sharp cooling events as compared to climate model simulations (Fig. 3), this may provide some constraints on the extent and duration of FWF from the Antarctic ice sheet.

4-4: Implications for climate system changes at high southern latitudes

Reconstructions have suggested that changes in Southern Ocean circulation, probably driven by wind changes, were important for the modulation of Southern Ocean CO_2 outgassing during the deglaciation. Proxies suggest an enhanced opal flux during HS1, which could reflect increased upwelling in the Southern Ocean due to changes in Southern Hemispheric westerlies (SHW) (Anderson et al., 2009), and poleward shift of the SHW across the deglaciation (Gray et al., 2023). Proxies also suggest decreasing deep and intermediate-depth Southern Ocean ventilation ages (Skinner et al., 2010, Burke et al., 2011), increasing intermediate-depth pH in the Southern Ocean during HS1 (Rae et al., 2018). It has been

suggested that stronger or poleward-shifted SHW and/or enhanced AABW formation during HS1 would indeed enhance Southern Ocean CO_2 outgassing and lead to an atmospheric CO_2 increase (Menviel et al., 2014; Menviel et al., 2018). In contrast, in the present study, most models show very little change or a gradual weakening in the SHW across the deglaciation, and there is little latitudinal migration of the SHW. Only the HadCM3 model displays a SHW strengthening during HS1. Biases in the SHW in PI simulations can be a cause of little changes in SHW, however, additional studies should look in more details into potential changes in the SHW in these simulations, as well as regional changes in SHW strength and their relation to other climatic variables (Rojas et al., 2009; Sime et al., 2013). In addition, no model exhibits an increase in AABW formation, which could contribute to the upwelling of carbon-rich waters and CO_2 outgassing from the Southern Ocean. Instead, the long-term AABW weakening by Southern Ocean warming and sea ice melt are consistent with previous analysis of deglaciation experiments (Marson et al., 2016). While it has been suggested that larger Southern Ocean sea ice extent would lead to an atmospheric CO_2 decrease at the LGM (Ferrari et al., 2014; Marzocchi et al., 2020, Stein et al., 2020), few models simulate significant changes in atmospheric CO_2 due to Southern Ocean sea ice change (Gottschalk et al., 2019). These physical changes still need to be reconciled with processes put forward to explain the deglacial atmospheric CO_2 changes by running coupled climate-carbon simulations.

Finally, we also find that changes in subsurface ocean temperature in the Southern Ocean, one of the critical factors impacting the retreat of the Antarctic ice sheet, display significant differences across the simulations. This could be related to different ECS or FWF in the Southern Ocean, and should also be investigated in future studies to quantify uncertainties in subsurface ocean temperature changes. Model-dependent subsurface ocean temperature change is one source of uncertainty in projecting future Antarctic ice sheet mass loss (Serrousi et al., 2020). In contrast to the present simulations of the last deglaciation, which prescribe the Antarctic ice sheet history, climate variability occurring during the deglaciation can impact the Antarctic ice sheet, which can act as feedback to Southern Ocean climate via meltwater input from the Antarctic ice sheet (Menviel et al., 2010; Golledge et al., 2014; Clark et al., 2020). Hence, further coupled climate and ice sheet modelling studies are needed to improve our understanding of climatological and glaciological processes and to evaluate model performance under a warming climate and rising sea levels (Gomez et al., 2020).

5. Conclusion

In our multi-model analysis of transient deglacial experiments, the early increase in Antarctic SAT is weakly simulated or absent. The multi-model difference could be related to differences in LGM sea ice extent, which may affect the sensitivity to insolation change, or to a slight reduction in the AMOC in response to small freshwater input from NH ice sheets. In addition, the different warming rates between West and East Antarctica suggested by ice core records are not reproduced by the transient simulations. In all models, a major warming occurs at southern high latitudes between 18 and 15 ka in response to increased CO_2 concentration. The multi-model analysis and sensitivity experiments further suggest that the AMOC reduction during HS1 associated with increased freshwater flux in the North Atlantic contributes to a larger warming in southern high latitudes, in agreement with high southern latitude proxy records, even though no simulation can reproduce both the amplitude of Southern Ocean SST and Antarctic SAT changes simultaneously. The bipolar seesaw model indicates that all models have a bipolar seesaw response, and that an abrupt AMOC increase at the end of HS1 is necessary to simulate the high southern latitude cooling during the BA (corresponding to the ACR). The simulations exhibit little changes in winds over the Southern Ocean and meridional circulation in the Southern Ocean, thus questioning the processes that could have contributed to enhanced CO_2 outgassing from the Southern Ocean. This indicates the necessity for future climate system modelling studies to quantify the sequence of deglacial climate changes and atmospheric CO_2 increase.

Acknowledgements:

We thank the two anonymous referees for their valuable comments which have substantially improved our paper. TO, AAO, TV and WLC acknowledge funding from JSPS Kakenhi 17H06104, 17H06323, and JPJSBP120213203. TO was also supported by JPMXD0722680395 and JSPS Kakenhi 24H00026. We acknowledge discussions at PAGES-QUIGS T5–T0 workshops, supported by INQUA Terminations Five to Zero (T5–T0) Working Group (Project #2004). LM acknowledges funding from Australian Research Council (ARC) grants FT180100606 and SR200100008. UM and MK acknowledge funding by the German Federal Ministry of Education and Research as a Research for Sustainability Initiative through the PalMod project (grant nos. 01LP1915C, and 01LP1917B). The MLR analysis used

scikit-learn library of Python 3.7. The figures were created using Generic Mapping Tool (GMT version 4 and 6).

Data availability:

All model data supporting our findings will be archived at Zenodo. Original model data is upon request for authors from each modelling group.

Code availability:

The bipolar seesaw model and the MLR model used in this study can be shared upon request.

Author contribution:

TO, LM, and AAO conceived the study. TO, LM, TV, BS analysed the data. TO, LM, AAO, TV, RI, and BS wrote the manuscript with input from all co-authors.

Competing interests:

Laurie Menviel is a member of the editorial board of Climate of the Past, but otherwise all authors declare that they have no conflict of interest.

References:

Name	Climate model name	Equilibrium Climate Sensitivity (ECS) [K]	Global mean LGM SAT anomaly [K]	References
iTRACE	iCESM1.3	3.6	7.3	Tierney et al., (2020)
LOVECLIM	LOVECLIM	2.8	4.2	McDougall et al., (2020), Goosse et al., (2010)
MIROC	MIROC4m	3.9	4.5	Chan and Abe-Ouchi, (2020)
HadCM3	HadCM3B	2.7	6.1	Kageyama et al., (2021)
MPI-ESM	MPI-ESM-CR P2		6.1	Kapsch et al., (2022)
iLOVECLIM	iLOVECLIM	2.0	3.5	Bouttes et al., (2023)

Table 1: Summary of climate models analysed in this study. Note that the ECS for MPI-ESM (model version MPI-ESM-CR P2) has not been calculated.

Name	Freshwater scheme	GHGs	Ice sheets	References for deglaciation experiments
iTRACE	TraCE-like	PMIP4	ICE-6G_C	He et al., 2019; 2021
LOVECLIM	TraCE-like, spatially uniform to the North Atlantic	Kohler et al., 2017	ICE-5G	Menviel et al., 2011
MIROC	ICE-6G_C with adjustment, spatially uniform to the North Atlantic	PMIP4	ICE-5G (LGM fix)	Obase and Abe-Ouchi 2019; Obase et al., 2021
HadCM3	ICE-6G_C	PMIP4	Ice-6G_C	Ivanovic et al., 2018; Snoll et al., 2022
MPI-ESM	ICE-6G_C	Kohler et al., 2017	Ice-6G_C	Kapsch et al., 2022
iLOVECLIM	ICE-6G_C	PMIP4	Ice-6G_C	Bouttes et al., 2023

Table 2: Summary of the experimental design used in the transient deglacial simulations. PMIP4 in the column GHGs indicates they use three GHGs reconstructions (CO_2, CH_4, N_2O) in PMIP4 protocol paper (Ivanovic et al., 2016)

	CO_2 coefficient [K/83 ppm]	AMOC coefficient [K/(normalised AMOC)]	Coefficient of Determination
iTRACE	6.5	–2.4	0.90
LOVECLIM	4.1	–0.4	0.91
MIROC	1.4	–0.5	0.81
HadCM3	3.3	–1.4	0.95
MPI-ESM	3.1	–1.2	0.90

iLOVECLIM	1.0	–1.4	0.56

Table 3: Results of the MLR model for Southern Ocean SST.

Parameter [unit]	Range
CO_2 coefficient α [K/83 ppm]	1.0–7.0, every 0.2
AMOC coefficient β [K/(normalised AMOC)]	0.0–3.0, every 0.1
Response timescale τ [year]	100–1000, every 100

Table 4: Parameter ranges in the thermal bipolar seesaw model.

	CO_2 coefficient [K/83 ppm]	AMOC coefficient [K/(normalised AMOC)]	Response timescale [year]	Coefficient of determination
iTRACE	6.0	–2.9	500	0.97
LOVECLIM	4.4	–0.6	300	0.94
MIROC	2.4	–0.9	600	0.97
HadCM3	4.8	–1.3	700	0.99
MPI-ESM	3.4	–1.4	500	0.95
iLOVECLIM	2.0	–0.8	100	0.54

Table 5: Results of the bipolar seesaw model for Southern Ocean SST

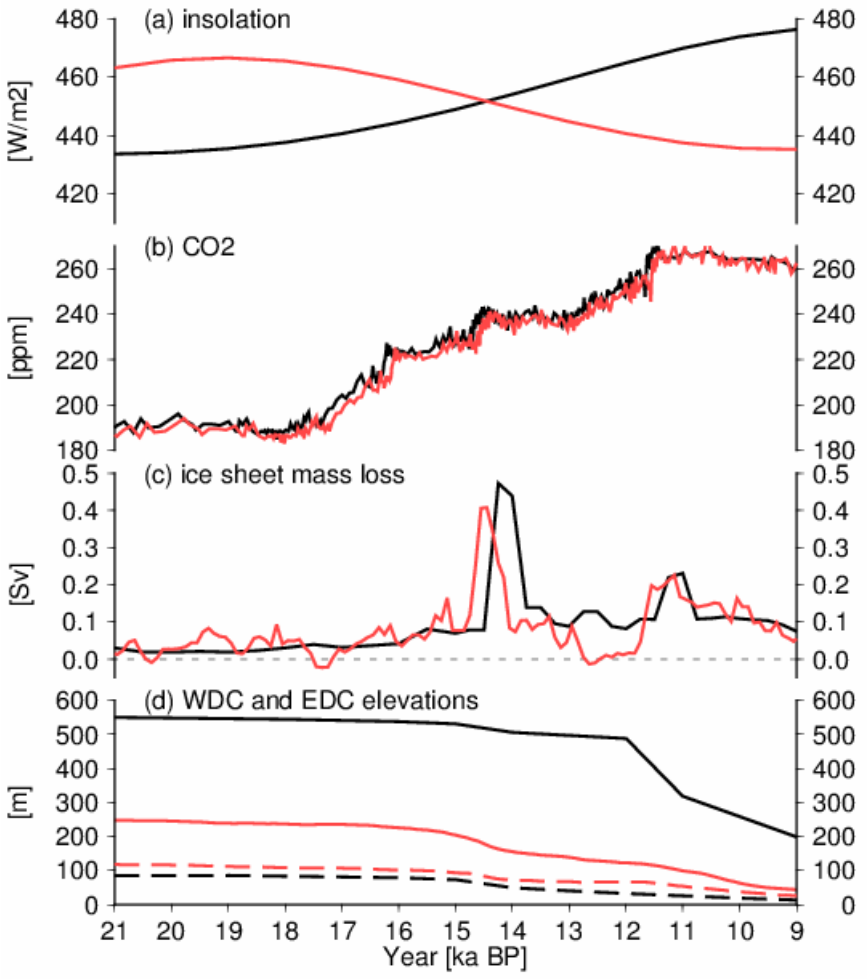

Figure 1: Forcing of the last deglaciation. (a) Insolation based on Berger (1978). Black: 65°N July, red: 65°S January, (b) CO_2. Black: Bereiter et al., (2015), red: Kohler et al., (2017), (c) FWF in the NH from ICE-6G_C (black lines) and GLAC-1D (red lines), (d) Elevation change at WDC (bold lines) and EDC (dashed lines) from ICE-6G_C (black lines) and GLAC-1D (red lines).

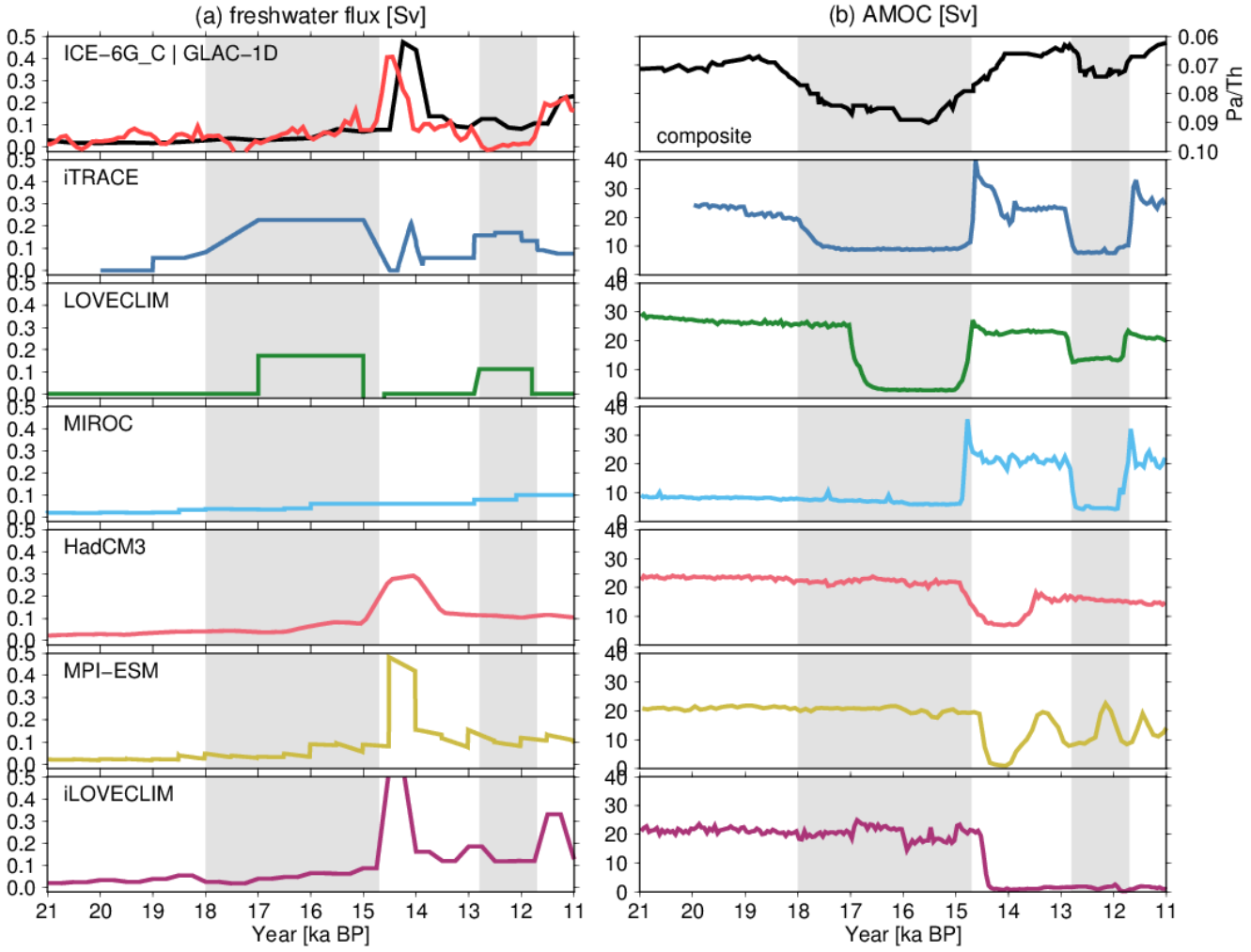

Figure 2: (a) Freshwater forcing (total value in the NH) and (b) simulated AMOC time series. The top panels indicate the freshwater flux from ice sheet reconstructions (black indicates ICE-6G_C and red indicates GLAC-1D) and composite $^{231}Pa/^{230}Th$ in the North Atlantic, retrieved from Ng et al., (2018). The top three model panels correspond to the first group with FWF adjusted to reproduce large-scale AMOC variability, and the bottom three model panels correspond to the second group with FWF consistent with the reconstructed ice volume changes. The grey shading indicates HS1 (18–14.7 ka) and the YD (12.8–11.7 ka), respectively, and the period in between corresponds to the BA (14.7–12.8 ka). .

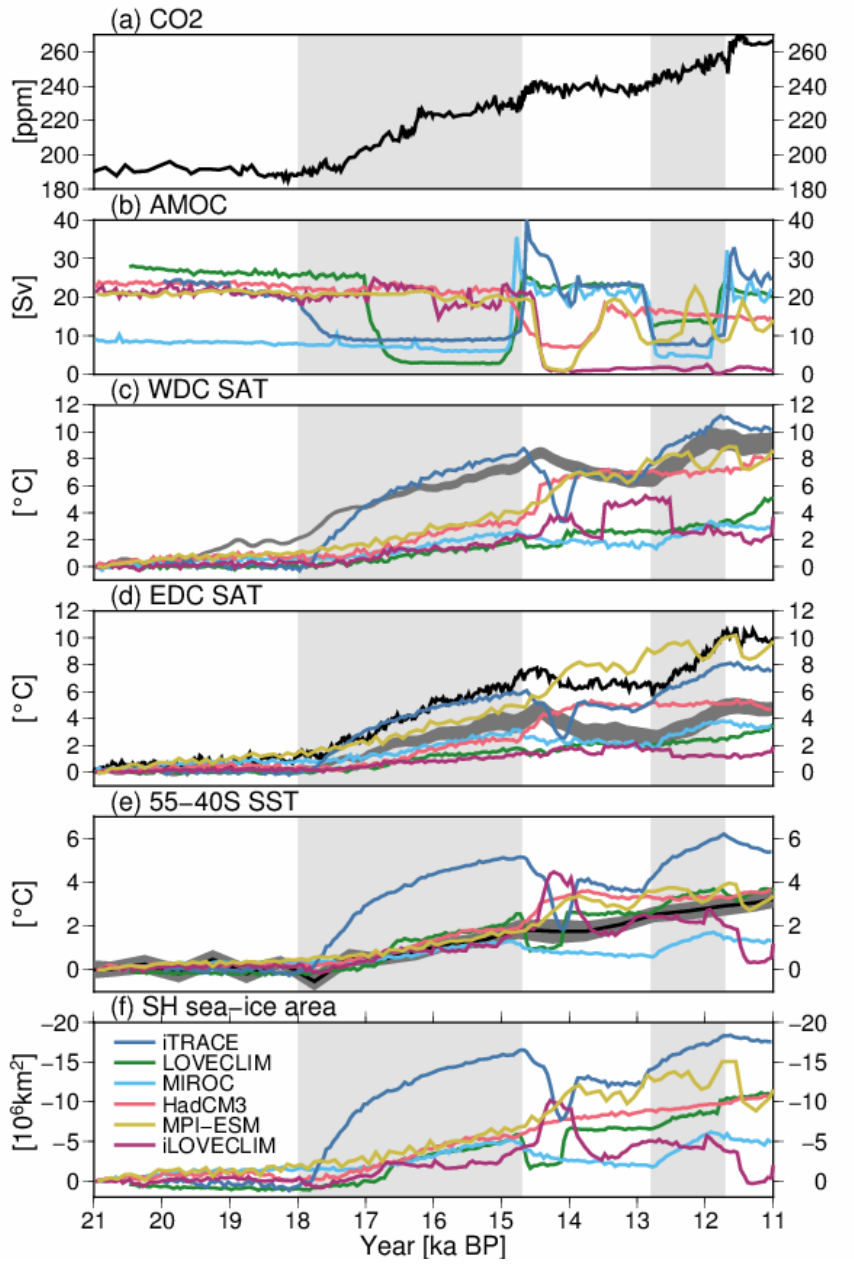

Figure 3: Time series of (a) atmospheric CO_2 (Bereiter et al., 2015) and (b) simulated AMOC, (c–d) SAT at WDC and EDC, (e) Southern Ocean SST (zonal mean SST in the latitude band 55–40°S), (f) Southern Ocean sea ice area in the transient simulations. The SAT, SST and sea ice area indicate changes since the LGM. The grey lines in (c–d) represent reconstructions from Buizert et al., (2013), and the black line in (d) represents reconstructions from Parrenin et al., (2013). The black lines and grey shades in (e) indicate the Southern Ocean SST stack and its standard error, respectively, as derived by Anderson et al., (2020).

The vertical grey shading indicates HS1 (18–14.7 ka) and the YD (12.8–11.7 ka), respectively, and the period in between corresponds to the BA (14.7–12.8 ka).

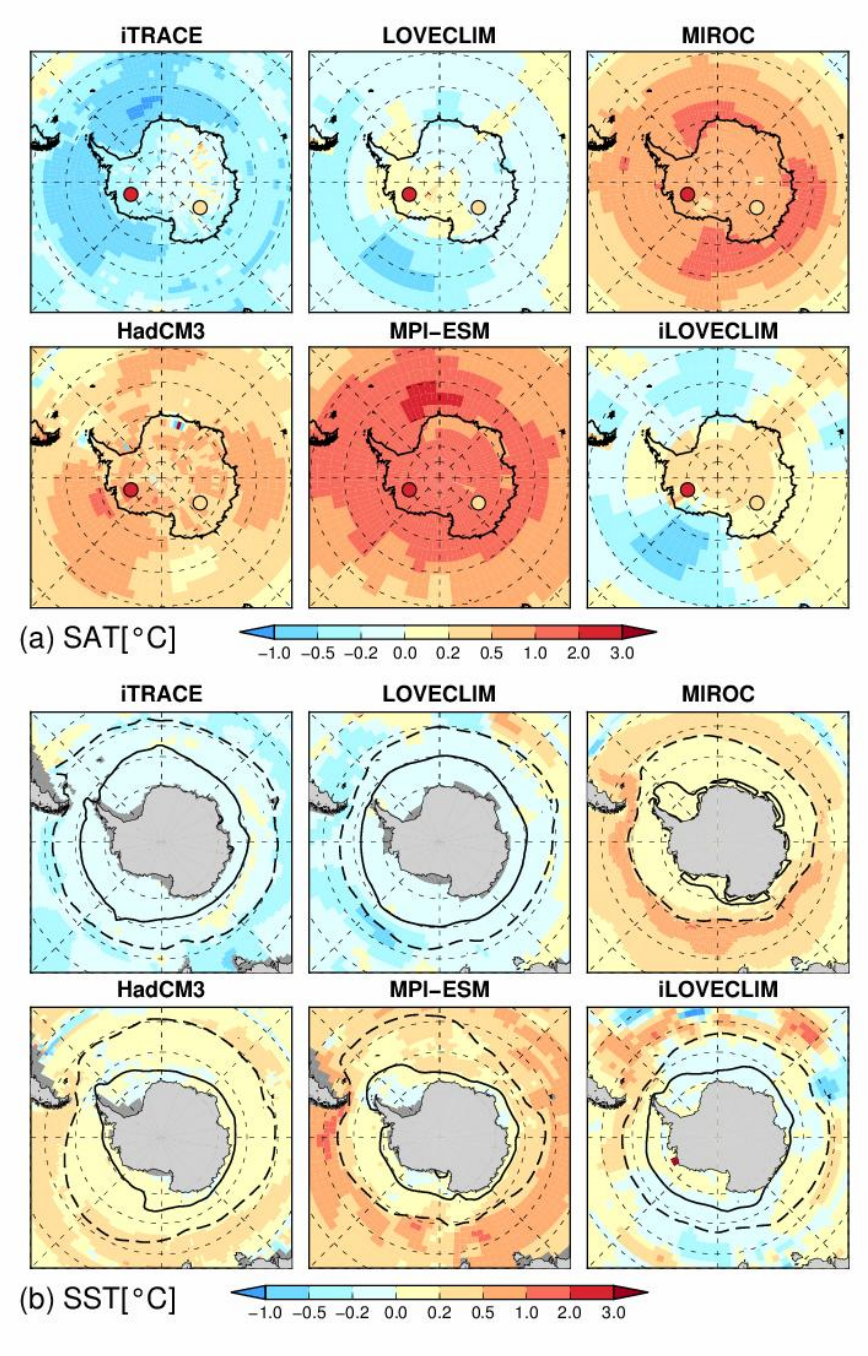

Figure 4: (a) SAT and (b) SST anomalies at 18 ka compared to the LGM. The coloured circles in (a) represent 18 ka-LGM SAT change based on ice core data (Parrenin et al., 2013), and the bold and dashed lines in (b) represent LGM austral summer and winter sea ice extent (85 and 15% annual-mean sea ice concentration), respectively.

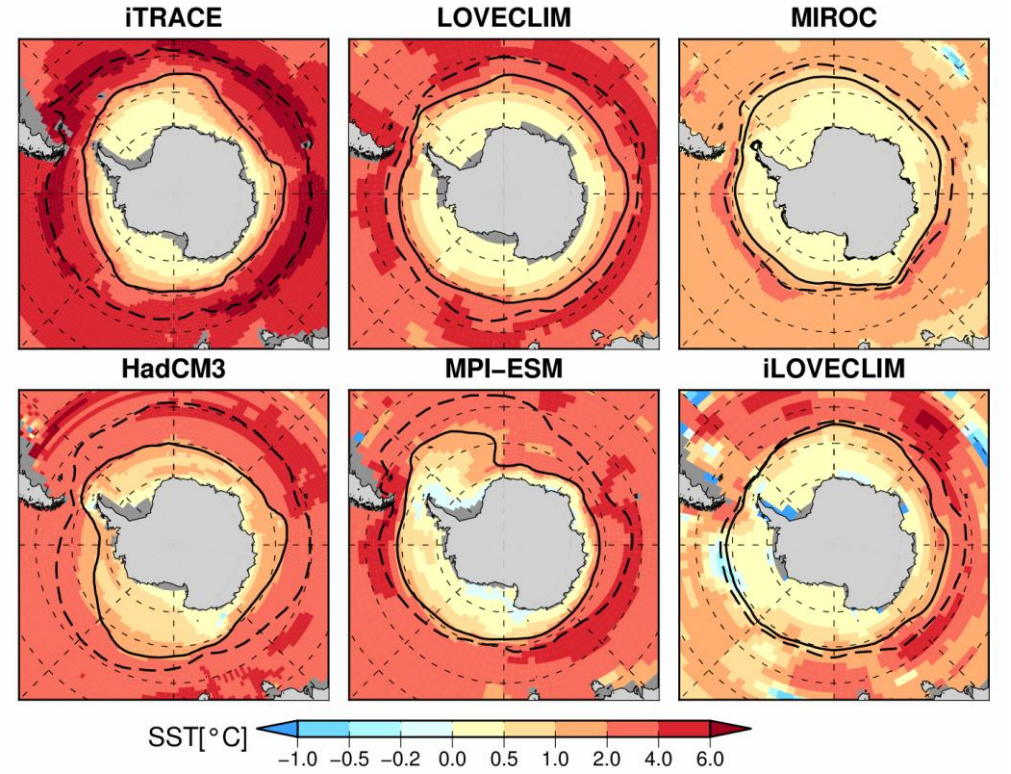

Figure 5: SST anomalies at 11 ka compared to the LGM. The bold and dashed lines indicate LGM and 11 ka sea ice extent (15% sea ice concentration), respectively.

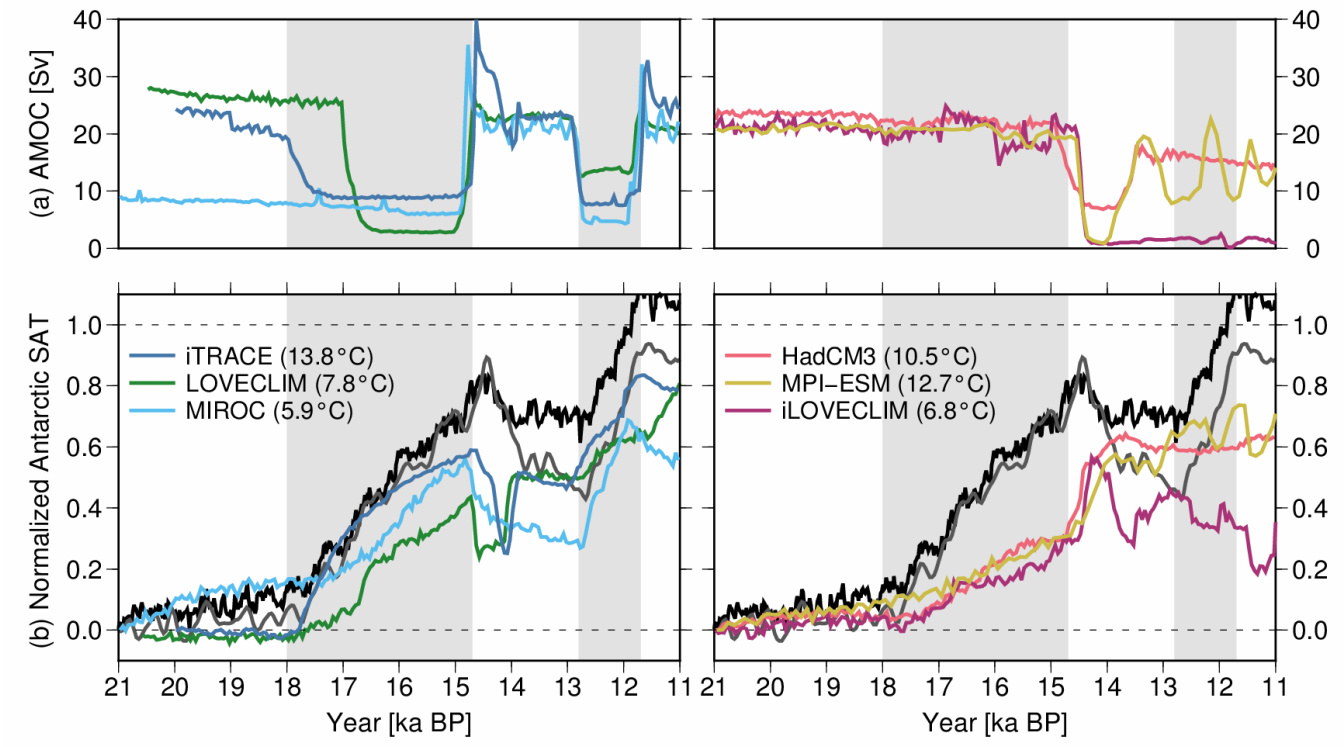

Figure 6: AMOC and normalised Antarctic SAT, with respect to the difference between PI and LGM. The actual PI and LGM differences are indicated in parentheses. The left panels show three simulations with weak AMOC during HS1, and the right show strong AMOC during HS1, respectively. The grey and black lines in (b) is normalised Antarctic SAT from EDC based on Parrenin et al., (2013) and Buizert et al., (2021), respectively. The vertical grey shading indicates HS1 (18–14.7 ka) and the YD (12.8–11.7 ka), respectively, and the period in between corresponds to the BA (14.7–12.8 ka).

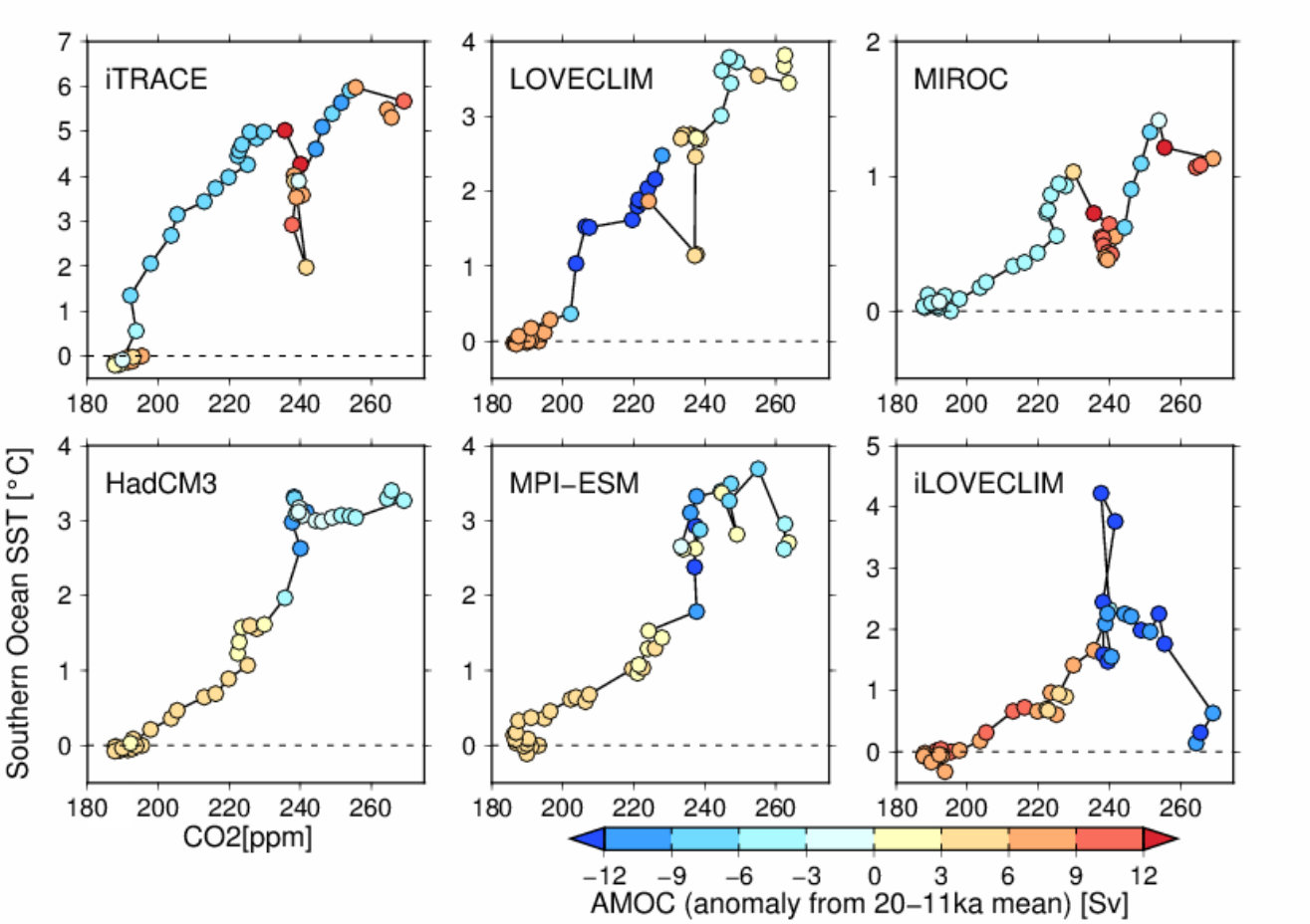

Figure 7: Relationship between Southern Ocean SST (vertical axis, change since LGM), CO_2 (horizontal axis) and AMOC strength anomaly from the mean strength between 20–11 ka (colours). The trajectory of the deglacial CO_2 forcing (CO_2), simulated SST changes and AMOC are plotted with circles at 200-year intervals. Note that the vertical axes are different between models to represent the total deglacial warming.

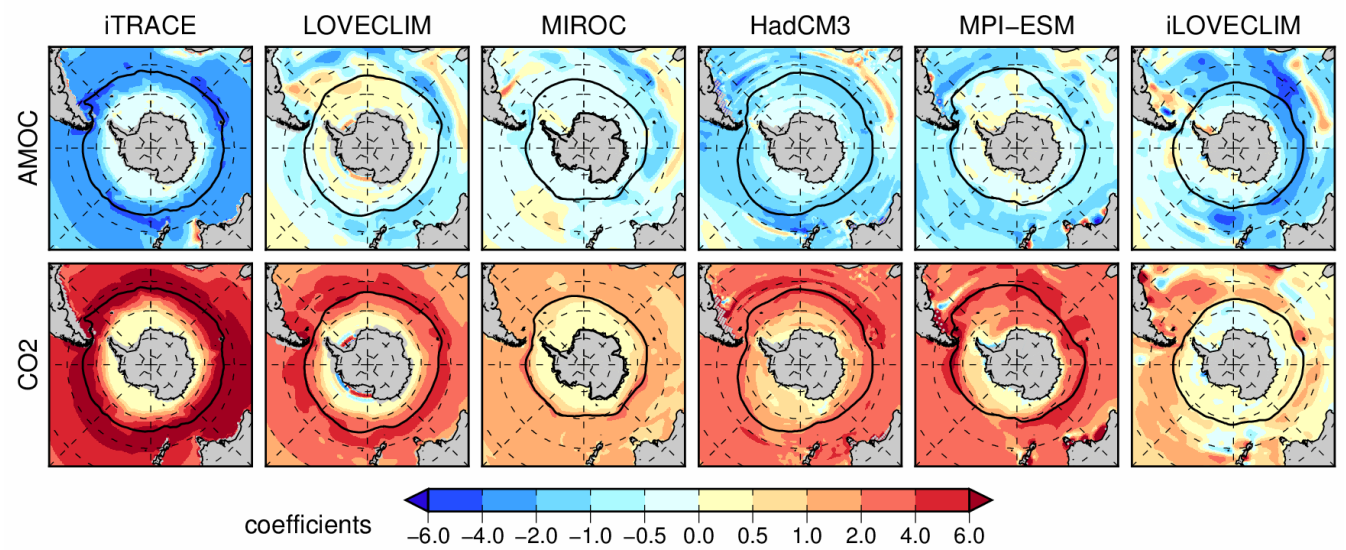

Figure 8: Results of the MLR model for 2-D SST maps. Top and bottom panels indicate AMOC [K/normalised AMOC] and CO_2 coefficients [K/83 ppm]. The black lines represent LGM winter sea ice edges.

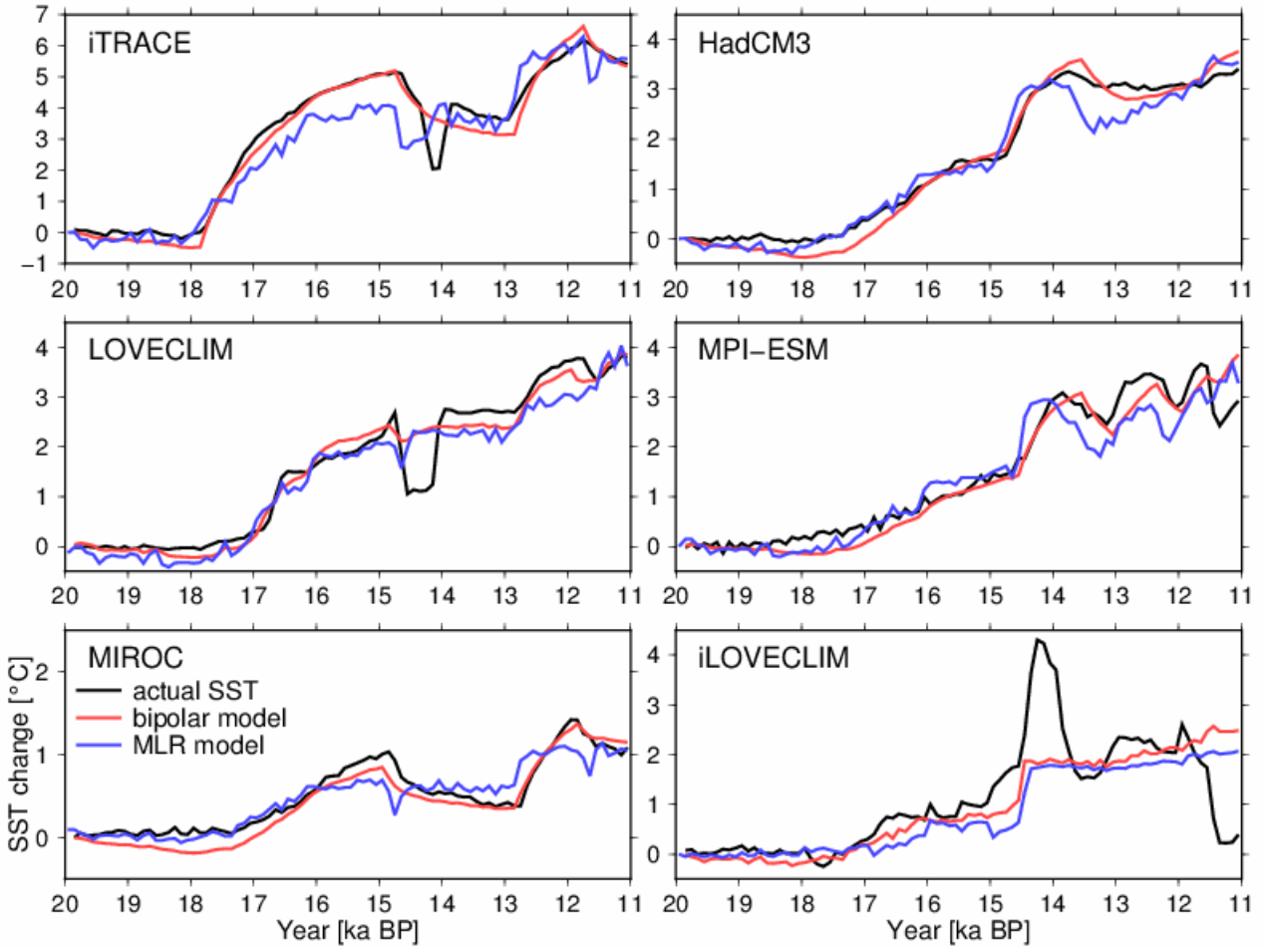

Figure 9: Results of the MLR model and bipolar seesaw model for Southern Ocean SST. The black lines represent the actual SST change (anomaly from 20 ka). The blue and red lines represent the results of MLR and bipolar seesaw models, respectively.

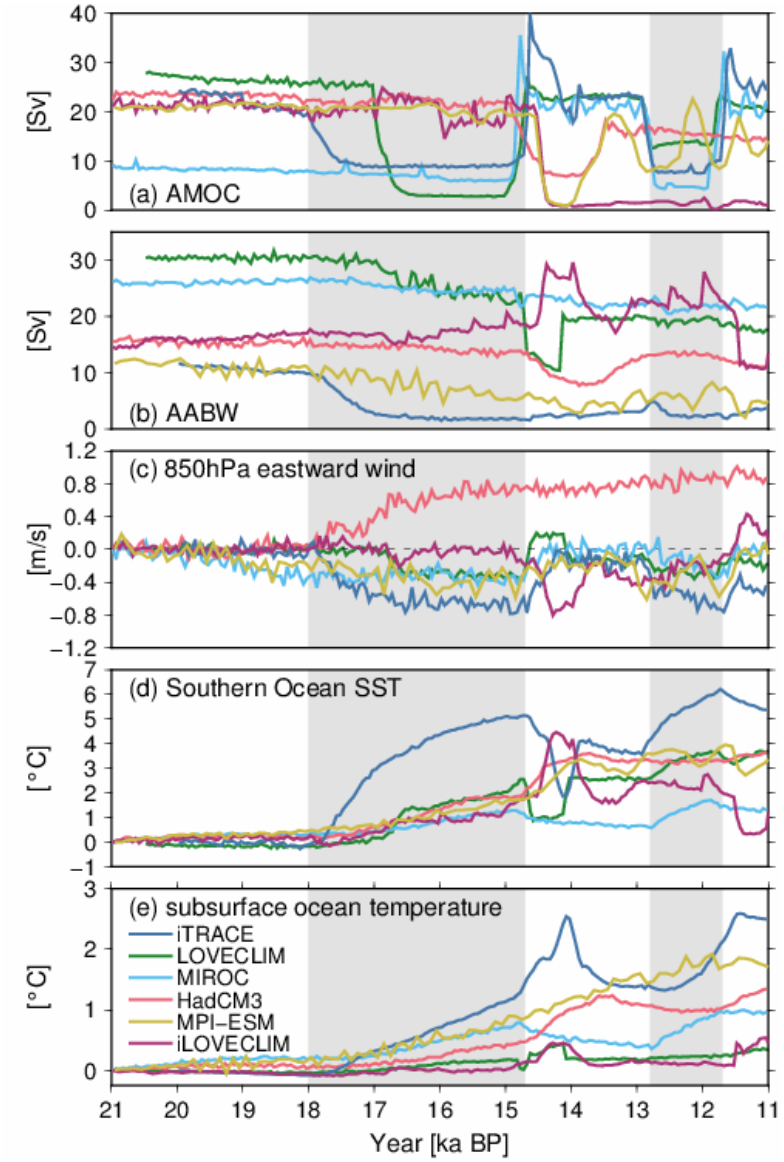

671

672 **Figure 10:** Time series of simulated (a) AMOC, (b) AABW, (c) 850 hPa eastward winds over the
673 Southern Ocean (65–40°S), (d) Southern Ocean SST, and (e) subsurface ocean temperature south of 60°S
674 (at depths 400–666m). The vertical grey shading indicates HS1 (18–14.7 ka) and the YD (12.8–11.7 ka),
675 respectively, and the period in between corresponds to the BA (14.7–12.8 ka).

676

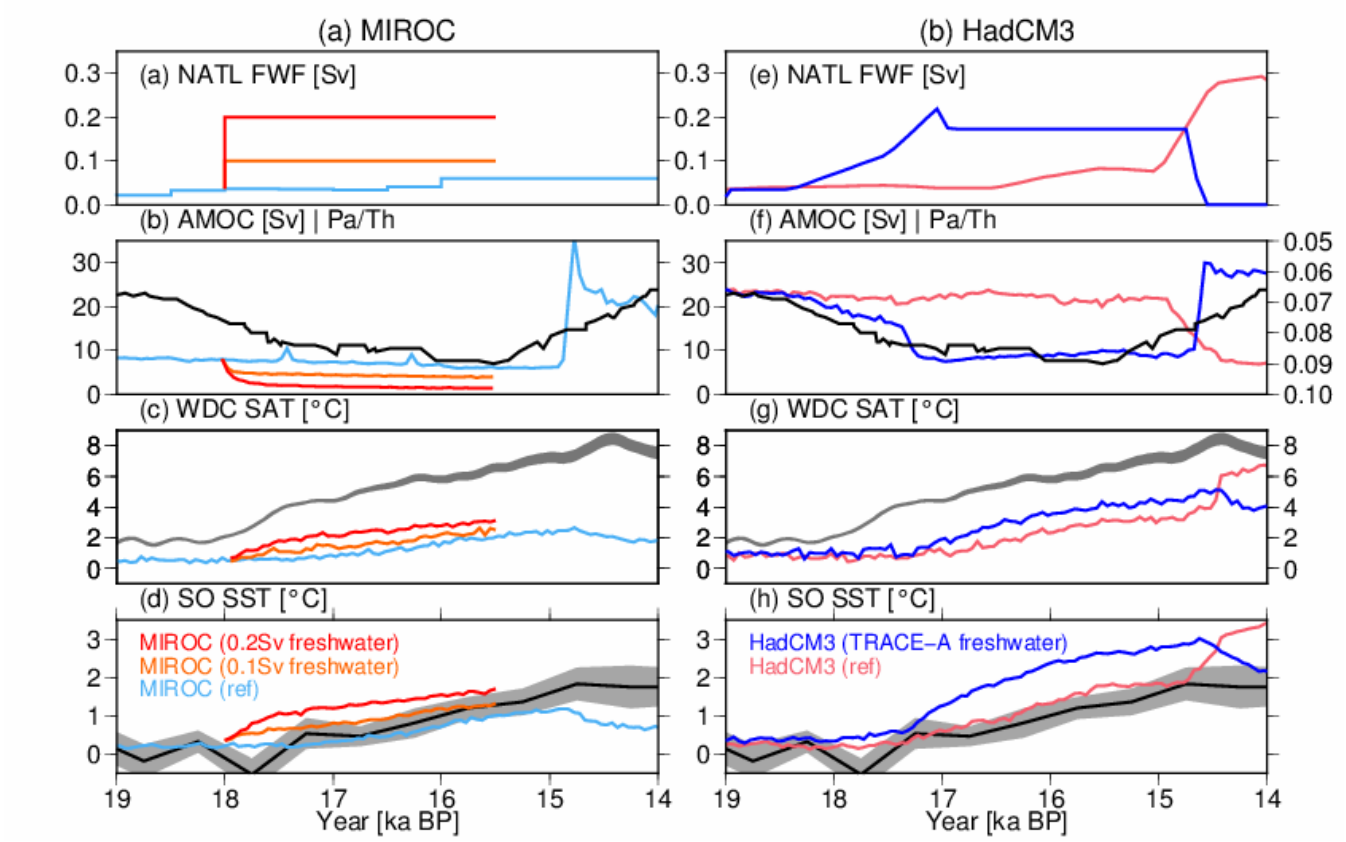

Figure 11: Results from transient deglaciation experiments performed with (a) MIROC and (b) HadCM3. The black lines in each panel represent the same proxy data as in Figure 3 (Parrenin et al., 2013: Buizert et al., 2021; Anderson et al., 2020). In two MIROC sensitivity experiments, a larger amount of freshwater flux (0.1 or 0.2 Sv) is added into the North Atlantic (50–70°N) during 18-15.5 ka compared to the standard MIROC experiment (light blue lines). In the TRACE-A HadCM3 sensitivity experiment (blue lines), a larger freshwater flux is added in the North Atlantic following the Trace-21ka simulation (Liu et al., 2009), while the pink lines in (b) represent the HadCM3 simulation used in Snoll et al. (2022).

References

1. Abe-Ouchi, A., Saito, F., Kawamura, K., Raymo, M. E., Okuno, J., Takahashi, K., and Blatter, H.: Insolation-driven 100,000-year glacial cycles and hysteresis of ice-sheet volume. Nature 500, 190–193, doi: 10.1038/nature12374, 2013

2. Abe-Ouchi, A., Saito, F., Kageyama, M., Braconnot, P., Harrison, S. P., Lambeck, K., Otto-Bliesner, B. L., Peltier, W. R., Tarasov, L., Peterschmitt, J.-Y., and Takahashi, K.: Ice-sheet configuration in the CMIP5/PMIP3 Last Glacial Maximum experiments, Geosci. Model Dev., 8, 3621?3637, doi:10.5194/gmd-8-3621-2015, 2015.
3. Anderson, B. E., & Burckle, L. H.: Rise in Atmospheric CO2. Science, 323 (March), 1443–1448, 2009
4. Anderson, H. J., Pedro, J. B., Bostock, H. C., Chase, Z., and Noble, T. L.: Compiled Southern Ocean sea surface temperatures correlate with Antarctic Isotope Maxima, Quaternary Science Reviews, 255, 106821, https://doi.org/10.1016/j.quascirev.2021.106821, 2021.
5. Anderson, Harris J; Pedro, Joel B; Bostock, Helen C; Chase, Zanna; Noble, Taryn L (2020): Southern Ocean Sea Surface Temperature Anomaly Stacks [dataset]. PANGAEA, https://doi.org/10.1594/PANGAEA.912158
6. Annan, J. D., Hargreaves, J. C., and Mauritsen, T.: A new global surface temperature reconstruction for the Last Glacial Maximum, Clim. Past, 18, 1883–1896, https://doi.org/10.5194/cp-18-1883-2022, 2022.
7. Bentley, M. J., Ocofaigh, C., Anderson, J. B., Conway, H., Davies, B., Graham, A. G. C., Hillenbrand, C. D., Hodgson, D. A., Jamieson, S. S. R., Larter, R. D., Mackintosh, A., Smith, J. A., Verleyen, E., Ackert, R. P., Bart, P. J., Berg, S., Brunstein, D., Canals, M., Colhoun, E. A., Crosta, X., Dickens, W. A., Domack, E., Dowdeswell, J. A., Dunbar, R., Ehrmann, W., Evans, J., Favier, V., Fink, D., Fogwill, C. J., Glasser, N. F., Gohl, K., Golledge, N. R., Goodwin, I., Gore, D. B., Greenwood, S. L., Hall, B. L., Hall, K., Hedding, D. W., Hein, A. S., Hocking, E. P., Jakobsson, M., Johnson, J. S., Jomelli, V., Jones, R. S., Klages, J. P., Kristoffersen, Y., Kuhn, G., Leventer, A., Licht, K., Lilly, K., Lindow, J., Livingstone, S. J., Massé, G., McGlone, M. S., McKay, R. M., Melles, M., Miura, H., Mulvaney, R., Nel, W., Nitsche, F. O., O'Brien, P. E., Post, A. L., Roberts, S. J., Saunders, K. M., Selkirk, P. M., Simms, A. R., Spiegel, C., Stolldorf, T. D., Sugden, D. E., van der Putten, N., van Ommen, T., Verfaillie, D., Vyverman, W., Wagner, B., White, D. A., Witus, A. E., and Zwartz, D.: A community-based geological reconstruction of Antarctic Ice Sheet deglaciation since the Last

Glacial Maximum, Quaternary Sci. Rev., 100, 1–9, https://doi.org/10.1016/j.quascirev.2014.06.025, 2014.

8. Berger, A.: Long-Term Variations of Daily Insolation and Quaternary Climatic Changes, J. Atmos. Sci., 35, 2362–2367, doi:10.1175/1520-0469(1978)035<2362:LTVODI>2.0.CO;2, 1978.
9. Bereiter, B., Eggleston, S., Schmitt, J., Nehrbass-Ahles, C., Stocker, T. F., Fischer, H., Kipfstuhl, S., and Chappellaz, J.: Revision of the EPICA Dome C CO2 record from 800 to 600 kyr before present, Geophys. Res. Lett., 42, 542–549, 10.1002/2014GL061957, 2015.
10. Bereiter, B., Shackleton, S., Baggenstos, D., Kawamura, K., and Severinghaus, J.: Mean global ocean temperatures during the last glacial transition. Nature, 553(7686), 39–44. https://doi.org/10.1038/nature25152, 2018.
11. Bethke, I., Li, C., and Nisancioglu, K. H.: Can we use ice sheet reconstructions to constrain meltwater for deglacial simulations? Paleoceanography, 27 (November 2011), 1–17. doi:10.1029/2011PA002258, 2012
12. Böhm, E., Lippold, J., Gutjahr, M., Frank, M., Blaser, P., Antz, B., Fohlmeister, J., Frank, N., Andersen, M. B. and Deininger, M.: Strong and deep Atlantic meridional overturning circulation during the last glacial cycle. Nature, 517(7534), 73–76. https://doi.org/10.1038/nature14059, 2015.
13. Bouttes, N., Roche, D. M., and Paillard, D.: Systematic study of the impact of fresh water fluxes on the glacial carbon cycle, Clim. Past, 8, 589–607, https://doi.org/10.5194/cp-8-589-2012, 2012.
14. Bouttes, N., Lhardy, F., Quiquet, A., Paillard, D., Goosse, H., and Roche, D. M.: Deglacial climate changes as forced by different ice sheet reconstructions, Clim. Past, 19, 1027–1042, https://doi.org/10.5194/cp-19-1027-2023, 2023.
15. Buizert, C., Gkinis, V., Severinghaus, J. P., He, F., Lecavalier, B. S., Kindler, P., Leuenberger, M., Carlson, A. E., Vinther, B., Masson-Delmotte, V., White, J. W. C., Liu, Z., Otto-Bliesner, B., and Brook, E. J.: Greenland temperature response to climate forcing during the last deglaciation, Science, 345, 1177–1180, 10.1126/science.1254961, 2014.
16. Buizert, C., Fudge, T. J., Roberts, W. H., Steig, E. J., Sherriff-Tadano, S., Ritz, C., Lefebvre, E., Edwards, J., Kawamura, K., Oyabu, I., Motoyama, H. Kahle, E. C., Jones, T. R., Abe-ouchi, A., Obase, T., Martin, C., Corr, H., Severinghaus, J. P., Beaudette, R. Epifanio, J. A., Brook, E. J., Martin,

K., Aoki, S., Nakazawa, T., Sowers, T. A., Alley, R. B., Ahn, J., Sigl, M., Severi, M., Dunbar, N. W., Svensson, A., Fegyveresi, J. M., He, C., Liu, Z., Zhu, J., Otto-bliesner, B. L., Lipenkov, V. Y., Kageyama, M., and Schwander, J.: Antarctic surface temperature and elevation during the Last Glacial Maximum, Science 372(6546), 1097-1101, doi: 10.1126/science.abd2897, 2021

17. Burke, A. and Robinson, L. F.: The Southern Ocean's Role in Carbon Exchange During the Last Deglaciation, Science, 135, 6068, 557-561. https://doi.org/10.1126/science.1208163, 2011
18. Capron, E., Landais, A., Chappellaz, J., Schilt, A., Buiron, D., Dahl-Jensen, D., Johnsen, S. J., Jouzel, J., Lemieux-Dudon, B., Loulergue, L., Leuenberger, M., Masson-Delmotte, V., Meyer, H., Oerter, H., and Stenni, B.: Millennial and sub-millennial scale climatic variations recorded in polar ice cores over the last glacial period, Clim. Past, 6, 345–365, https://doi.org/10.5194/cp-6-345-2010, 2010.
19. Chan, W.-L. and Abe-Ouchi, A.: Pliocene Model Intercomparison Project (PlioMIP2) simulations using the Model for Interdisciplinary Research on Climate (MIROC4m), Clim. Past, 16, 1523–1545, https://doi.org/10.5194/cp-16-1523-2020, 2020.
20. Clark, P. U., He, F., Golledge, N. R., Mitrovica, J. X., Dutton, A., Hoffman, J. S., and Dendy, S.:Oceanic forcing of penultimate deglacial and last interglacial sea-level rise. Nature, 577(7792), 660–664. https://doi.org/10.1038/s41586-020-1931-7, 2020
21. Condron, A., & Winsor, P.: Meltwater routing and the Younger Dryas. Proceedings of the National Academy of Sciences, 109(49), 19928–19933, https://doi.org/10.1073/pnas.1207381109, 2012
22. Crosta, X., Kohfeld, K. E., Bostock, H. C., Chadwick, M., Du Vivier, A., Esper, O., Etourneau, J., Jones, J., Leventer, A., Müller, J., Rhodes, R. H., Allen, C. S., Ghadi, P., Lamping, N., Lange, C. B., Lawler, K.-A., Lund, D., Marzocchi, A., Meissner, K. J., Menviel, L., Nair, A., Patterson, M., Pike, J., Prebble, J. G., Riesselman, C., Sadatzki, H., Sime, L. C., Shukla, S. K., Thöle, L., Vorrath, M.-E., Xiao, W., and Yang, J.: Antarctic sea ice over the past 130 000 years – Part 1: a review of what proxy records tell us, Clim. Past, 18, 1729–1756, https://doi.org/10.5194/cp-18-1729-2022, 2022.
23. Dansgaard, W., Johnsen, S. J., Clausen, H. B., Dahl-Jensen, D., Gundestrup, N. S., Hammer, C. U., Hvidberg, C. S., Steffensen, J. P., Sveinbjörnsdottir, A. E., Jouzel, J., and Bond, G.: Evidence for general instability of past climate from a 250-kyr ice-core record, Nature, 364, 218–220, https://doi.org/10.1038/364218a0, 1993

24. Deschamps, P., Durand, N., Bard, E., Hamelin, B., Camoin, G., Thomas, A. L., Henderson, G. M., Okuno, J., and Yokoyama, Y.: Ice-sheet collapse and sea-level rise at the Bølling warming 14,600 years ago, Nature, 28, 559–564, https://doi.org/10.1038/nature10902, 2012.
25. Ferrari, R., Jansen, M. F., Adkins, J. F., Burke, A., Stewart, A. L., and Thompson, A. F.: Antarctic sea ice control on ocean circulation in present and glacial climates, P. Natl. Acad. Sci. USA, 111, 8753–8758, 10.1073/pnas.1323922111, 2014.
26. Golledge, N., Menviel, L., Carter, L., Fogwill, C. J., England, M. H., Cortese, G., and Levy, R. H.: Antarctic contribution to meltwater pulse 1A from reduced Southern Ocean overturning. Nat Commun 5, 5107, https://doi.org/10.1038/ncomms6107, 2014.
27. Gomez, N., Weber, M. E., Clark, P. U., Mitrovica, J. X. and Han, H. K.: Antarctic ice dynamics amplified by Northern Hemisphere sea-level forcing, Nature, 587(7835), 600–604, doi:10.1038/s41586-020-2916-2, 2020
28. Goosse, H., Brovkin, V., Fichefet, T., Haarsma, R., Huybrechts, P., Jongma, J., Mouchet, A., Selten, F., Barriat, P.-Y., Campin, J.-M., Deleersnijder, E., Driesschaert, E., Goelzer, H., Janssens, I., Loutre, M.-F., Morales Maqueda, M. A., Opsteegh, T., Mathieu, P.-P., Munhoven, G., Pettersson, E. J., Renssen, H., Roche, D. M., Schaeffer, M., Tartinville, B., Timmermann, A., and Weber, S. L.: Description of the Earth system model of intermediate complexity LOVECLIM version 1.2, Geosci. Model Dev., 3, 603–633, https://doi.org/10.5194/gmd-3-603-2010, 2010.
29. Gottschalk, J., Battaglia, G., Fischer, H., Frölicher, T. L., Jaccard, S. L., Jeltsch-Thömmes, A., Joos, F., Köhler, P., Meissner, K. J., Menviel, L., Nehrbass-Ahles, C., Schmitt, J., Schmittner, A., Skinner, L. C., and Stocker, T. F.: Mechanisms of millennial-scale atmospheric CO2 change in numerical model simulations, Quaternary Sci. Rev., 220, 30–74, https://doi.org/10.1016/j.quascirev.2019.05.013, 2019.
30. Gray, W. R., de Lavergne, C., Willis, R. C. J., Menviel, L., Spence, P., Holzer, M., Kageyama, M. and Michel, E.: Poleward Shift in the Southern Hemisphere Westerly Winds Synchronous With the Deglacial Rise in CO2, Paleoceanography and Paleoclimatology, 38, 7, https://doi.org/10.1029/2023PA004666, 2023

31. Green, R. A., Menviel, L., Meissner, K. J., Crosta, X., Chandan, D., Lohmann, G., Peltier, W. R., Shi, X., and Zhu, J.: Evaluating seasonal sea-ice cover over the Southern Ocean at the Last Glacial Maximum, Clim. Past, 18, 845–862, https://doi.org/10.5194/cp-18-845-2022, 2022.
32. Gregoire, L. J., Payne, A. J., and Valdes, P. J.: Deglacial rapid sea level rises caused by ice-sheet saddle collapses, Nature, 487, 219–222, 10.1038/nature11257, 2012.
33. He, F., Shakun, J. D., Clark, P. U., Carlson, A. E., Liu, Z., Otto-Bliesner, B. L., and Kutzbach, J. E.: Northern Hemisphere forcing of Southern Hemisphere climate during the last deglaciation, Nature, 494, 81-85, https://doi.org/10.1038/nature11822, 2013.
34. He, C., Zhengyu Liu, and Aixue Hu,: The transient response of atmospheric and oceanic heat transports to anthropogenic warming. Nature Climate Change, 1, doi:10.1038/s41558-018-0387-3, 2019.
35. He, C., Liu, Z., Zhu, J., Zhang, J., Gu, S., Otto-Bliesner, B. L., Brady, E., Zhu, C., Jin, Y. and Sun, J.: North Atlantic subsurface temperature response controlled by effective freshwater input in "Heinrich" events, Earth and Planetary Science Letters, 539, 116247, https://doi.org/10.1016/j.epsl.2020.116247, 2020.
36. He, C., Liu, Z., Otto-Bliesner, B. L., Brady, E. C., Zhu, C., Tomas, R., Bao, Y.: Hydroclimate footprint of pan-Asian monsoon water isotope during the last deglaciation. Science Advances, 7(4), 1–12. https://doi.org/10.1126/sciadv.abe2611, 2021.
37. Hunter, S. J., Haywood, A. M., Dolan, A. M., and Tindall, J. C.: The HadCM3 contribution to PlioMIP phase 2, Clim. Past, 15, 1691–1713, https://doi.org/10.5194/cp-15-1691-2019, 2019.
38. Ivanovic, R. F., Gregoire, L. J., Kageyama, M., Roche, D. M., Valdes, P. J., Burke, A., Drummond, R., Peltier, W. R., and Tarasov, L.: Transient climate simulations of the deglaciation 21–9 thousand years before present (version 1) – PMIP4 Core experiment design and boundary conditions, Geosci. Model Dev., 9, 2563–2587, https://doi.org/10.5194/gmd-9-2563-2016, 2016.
39. Ivanovic, R. F., Gregoire, L. J., Burke, A., Wickert, A. D., and Valdes, P. J.: Acceleration of Northern Ice Sheet Melt Induces AMOC Slowdown and Northern Cooling in Simulations of the Early Last Deglaciation, Paleoceanography and Paleoclimatology. 807–824. doi:10.1029/2017PA003308, 2018

40. Jouzel, J., Masson-Delmotte, V., Cattani, O., Dreyfus, G., Falourd, S., Hoffmann, G., Minster, B., Nouet, J., Barnola, J. M., Chappellaz, J., Fischer, H., Gallet, J. C., Johnsen, S., Leuen- berger, M., Loulergue, L., Luethi, D., Oerter, H., Parrenin, F., Raisbeck, G., Raynaud, D., Schilt, A., Schwander, J., Selmo, E., Souchez, R., Spahni, R., Stauffer, B., Steffensen, J. P., Stenni, B., Stocker, T. F., Tison, J. L., Werner, M., and Wolff, E. W.: Orbital and Millennial Antarctic Climate Variability over the Past 800,000 Years, Science, 317, 793-796, https://doi.org/10.1126/science.1141038, 2007.
41. Kageyama, M., Merkel, U., Otto-Bliesner, B., Prange, M., Abe-Ouchi, A., Lohmann, G., Ohgaito, R., Roche, D. M., Singarayer, J., Swingedouw, D., and X Zhang: Climatic impacts of fresh water hosing under Last Glacial Maximum conditions: a multi-model study, Clim. Past, 9, 935–953, https://doi.org/10.5194/cp-9-935-2013, 2013.
42. Kageyama, M., Braconnot, P., Harrison, S. P., Haywood, A. M., Jungclaus, J. H., Otto-Bliesner, B. L., Peterschmitt, J.-Y., Abe-Ouchi, A., Albani, S., Bartlein, P. J., Brierley, C., Crucifix, M., Dolan, A., Fernandez-Donado, L., Fischer, H., Hopcroft, P. O., Ivanovic, R. F., Lambert, F., Lunt, D. J., Mahowald, N. M., Peltier, W. R., Phipps, S. J., Roche, D. M., Schmidt, G. A., Tarasov, L., Valdes, P. J., Zhang, Q., and Zhou, T.: The PMIP4 contribution to CMIP6 – Part 1: Overview and over- arching analysis plan, Geosci. Model Dev., 11, 1033–1057, https://doi.org/10.5194/gmd-11-1033-2018, 2018.
43. Kageyama, M., Harrison, S. P., Kapsch, M.-L., Lofverstrom, M., Lora, J. M., Mikolajewicz, U., Sherriff-Tadano, S., Vadsaria, T., Abe-Ouchi, A., Bouttes, N., Chandan, D., Gregoire, L. J., Ivanovic, R. F., Izumi, K., LeGrande, A. N., Lhardy, F., Lohmann, G., Morozova, P. A., Ohgaito, R., Paul, A., Peltier, W. R., Poulsen, C. J., Quiquet, A., Roche, D. M., Shi, X., Tierney, J. E., Valdes, P. J., Volodin, E., and Zhu, J.: The PMIP4 Last Glacial Maximum experiments: preliminary results and comparison with the PMIP3 simulations, Clim. Past, 17, 1065–1089, https://doi.org/10.5194/cp-17-1065-2021, 2021.
44. Kapsch, M.-L., Mikolajewicz, U., Ziemen, F. and Schannwell, C.: Ocean response in transient simulations of the last deglaciation dominated by underlying ice-sheet reconstruction and method of meltwater distribution, Geophysical Research Letters, 49, e2021GL096767, https://doi.org/10.1029/2021GL096767, 2022.

45. Kobayashi, H., Oka, A., Yamamoto, A., and Abe-Ouchi, A.: Glacial carbon cycle changes by Southern Ocean processes with sedimentary amplification. Science Advances, 7(35), doi: 10.1126/sciadv.abg7723, 2021.
46. Kobayashi, H., Oka, A., Obase, T., and Abe-Ouchi, A.: Assessing transient changes in the ocean carbon cycle during the last deglaciation through carbon isotope modeling, Clim. Past, 20, 769–787, https://doi.org/10.5194/cp-20-769-2024, 2024.
47. Kuniyoshi, Y., Abe-Ouchi, A., Sherriff-Tadano, S., Chan, W.-L., and Saito, F.: Effect of Climatic Precession on Dansgaard-Oeschger-Like Oscillations. Geophysical Research Letters, 49(6), e2021GL095695. https://doi.org/10.1029/2021GL095695, 2022.
48. Lambeck, K., Rouby, H., Purcell, A., Sun, Y., and Sambridge, M.: Sea level and global ice volumes from the Last Glacial Maximum to the Holocene, P. Natl. Acad. Sci., 111, 15296–15303, 10.1073/pnas.1411762111, 2014.
49. Lhardy, F., Bouttes, N., Roche, D. M., Crosta, X., Waelbroeck, C., and Paillard, D.: Impact of Southern Ocean surface conditions on deep ocean circulation during the LGM: a model analysis, Clim. Past, 17, 1139–1159, https://doi.org/10.5194/cp-17-1139-2021, 2021.
50. Lisiecki, L. E. and Raymo, M. E.: A Pliocene-Pleistocene stack of 57 globally distributed benthic d18O records, Paleoceanography, 20, PA1003, doi:10.1029/2004PA001071, 2005
51. Liu, Z., Otto-Bliesner, B. L., He, F., Brady, E. C., Tomas, R., Clark, P. U., Carlson, A. E., Lynch-Stieglitz, J., Curry, W., Brook, E., Erickson, D., Jacob, R., Kutzbach, J., and Cheng, J.: Transient Simulation of Last Deglaciation with a New Mechanism for Bølling-Allerød Warming, Science, 325, 310–314, doi:10.1126/science.1171041, 2009
52. Liu, Z., Bao, Y., Thompson, L. G., Mosley-Thompson, E., Tabor, C., Zhang, G. J., Yan, M., Lofverstrom, M., Montanez, I., and Oster, J.: Tropical mountain ice core δ18O: A Goldilocks indicator for global temperature change, Science Advances, 9, 45, https://doi.org/10.1126/sciadv.adi6725, 2023
53. Love, R., Andres, H. J., Condron, A., and Tarasov, L.: Freshwater routing in eddy-permitting simulations of the last deglacial: the impact of realistic freshwater discharge, Clim. Past, 17, 2327–2341, https://doi.org/10.5194/cp-17-2327-2021, 2021.

54. Lowry, D. P., Golledge, N. R., Menviel, L., and Bertler, N. A. N.: Deglacial evolution of regional Antarctic climate and Southern Ocean conditions in transient climate simulations. 189–215, 2018.
55. Lynch-Stieglitz, J., Adkins, J. F., Curry, W. B., Dokken, T., Hall, I. R., Herguera, J. C. and Zahn, R.: Atlantic meridional overturning circulation during the Last Glacial Maximum. Science, 316(5821), 66–69. https://doi.org/10.1126/science.1137127, 2007
56. MacDougall, A. H., Frölicher, T. L., Jones, C. D., Rogelj, J., Matthews, H. D., Zickfeld, K., Arora, V. K., Barrett, N. J., Brovkin, V., Burger, F. A., Eby, M., Eliseev, A. V., Hajima, T., Holden, P. B., Jeltsch-Thömmes, A., Koven, C., Mengis, N., Menviel, L., Michou, M., Mokhov, I. I., Oka, A., Schwinger, J., Séférian, R., Shaffer, G., Sokolov, A., Tachiiri, K., Tjiputra , J., Wiltshire, A., and Ziehn, T.: Is there warming in the pipeline? A multi-model analysis of the Zero Emissions Commitment from CO2, Biogeosciences, 17, 2987–3016, https://doi.org/10.5194/bg-17-2987-2020, 2020.
57. Marcott, S. A., Bauska, T. K., Buizert, C., Steig, E. J., Rosen, J. L., Cuffey, K. M., Fudge, T. J., Severinghaus, J. P., Kalk, M. L., McConnell, J. R., Sowers, T., Taylor, K. C. White, J. W. C. and Brook, E. J.: Centennial-scale changes in the global carbon cycle during the last deglaciation. Nature, 514(7524), 616–619. https://doi.org/10.1038/nature13799, 2014
58. Margari, V., Skinner, L. C., Menviel, L., Capron, E., Rhodes, R. H., Martrat, B., and Grimalt, J. O.: Fast and slow components of interstadial warming in the North Atlantic during the last glacial. Communications Earth & Environment, 1–9. https://doi.org/10.1038/s43247-020-0006-x, 2020
59. Mariotti, V., Paillard, D., Bopp, L., Roche, D. M., and Bouttes, N.: A coupled model for carbon and radiocarbon evolution during the last deglaciation. Geophysical Research Letters, 43(3), 1306–1313. https://doi.org/10.1002/2015GL067489, 2016.
60. Marson, J. M., Mysak, L. A., Mata, M. M., and Wainer, I.: Evolution of the deep Atlantic water masses since the last glacial maximum based on a transient run of NCAR-CCSM3. Climate Dynamics, 47(3–4), 865–877. https://doi.org/10.1007/s00382-015-2876-7, 2016
61. Martínez-Garcia, A., Rosell-Melé, A., Jaccard, S.: Southern Ocean dust–climate coupling over the past four million years. Nature 476, 312–315. https://doi.org/10.1038/nature10310, 2011.

62. Martrat, B., Grimalt, J. O., Shackleton, N. J., de Abreu, L., Hutterli, M.A., and Stocker, T. F.: Four climate cycles of recurring deep and surface water destabilizations on the Iberian Margin, Science, 317, 502–507, doi:10.1126/science.1139994, 2007.
63. Marzocchi, A. and Jansen, M. F. Global cooling linked to increased glacial carbon storage via changes in Antarctic sea ice. Nature Geoscience, 12, 1001–1005, https://doi.org/10.1038/s41561-019-0466-8, 2019
64. Masoum, A., Nerger, L., Willeit, M., Ganopolski, A., and Lohmann, G.: Lessons From Transient Simulations of the Last Deglaciation With CLIMBER-X: GLAC1D Versus PaleoMist, Geophysical Research Letters, 51(16), e2023GL107310. https://doi.org/10.1029/2023GL107310, 2024.
65. McManus, J. F., Francois, R., Gherardi, J.-M., Keigwin, L. D., and Brown-Leger, S.: Collapse and rapid resumption of Atlantic meridional circulation linked to deglacial climate changes, Nature, 428, 834–837, 10.1038/nature02494, 2004.
66. Menviel, L., Yu, J., Joos, F., Mouchet, A., Meissner, K. J., and England, M. H.: Poorly ventilated deep ocean at the Last Glacial Maximum inferred from carbon isotopes: A data-model comparison study. Paleoceanography, 32(1), 2–17. https://doi.org/10.1002/2016PA003024, 2017.
67. Menviel, L., Timmermann, a., Timm, O. E., and Mouchet, A.: Climate and biogeochemical response to a rapid melting of the West Antarctic Ice sheet during interglacials and implications for future climate. Paleoceanography, 25, 1–12. https://doi.org/10.1029/2009PA001892, 2010.
68. Menviel, L., Timmermann, A., Timm, O. E., and Mouchet, A.: Deconstructing the Last Glacial termination: the role of millennial and orbital-scale forcings, Quaternary Sci. Rev., 30, 1155–1172, 10.1016/j.quascirev.2011.02.005, 2011.
69. Menviel, L., England, M. H., Meissner, K. J., Mouchet, A., and Yu, J.: Atlantic-Pacific seesaw and its role in outgassing CO2 during Heinrich events. Paleoceanography, 29(January), 58–70. https://doi.org/10.1002/2013PA002542, 2014.
70. Menviel, L., Spence, P., Yu, J., Chamberlain, M. A., Matear, R. J., Meissner, K. J., and England, M. H.: Southern Hemisphere westerlies as a driver of the early deglacial atmospheric CO2 rise. Nature Communications, 9(1), 1–12. https://doi.org/10.1038/s41467-018-04876-4, 2018

71. Moros, M., De Deckker, P., Perner, K., Ninnemann, U. S., Wacker, L., Telford, R., Jansen, E., Blanz, T. andSchneider, R.: Hydrographic shifts south of Australia over the last deglaciation and possible interhemispheric linkages. Quaternary Research (United States), 102, 130–141. https://doi.org/10.1017/qua.2021.12, 2021
72. Morrison, A. and Hogg, A.: On the Relationship between Southern Ocean Overturning and ACC Transport, J. Phys. Oceanogr., 43, 140–148, 2013.
73. Moy, A. D., Palmer, M. R., Howard, W. R., Bijma, J., Cooper, M. J., Calvo, E., Pelejero, C., Gagan, M. K. and Chalk, T. B.: Varied contribution of the Southern Ocean to deglacial atmospheric CO2 rise. Nature Geoscience, 12(12), 1006–1011. https://doi.org/10.1038/s41561-019-0473-9, 2019
74. Ng, H. C., Robinson, L. F., McManus, J. F., Mohamed, K. J., Jacobel, A. W., Ivanovic, R. F., Gregoire, L. J.and Chen, T.: Coherent deglacial changes in western Atlantic Ocean circulation. Nature Communications, 9(1), 1–10. https://doi.org/10.1038/s41467-018-05312-3, 2018
75. Obase, T., and Abe- Ouchi, A.: Abrupt Bølling-Allerød warming simulated under gradual forcing of the last deglaciation, Geophysical Research Letters, 46, https://doi.org/10.1029/2019GL084675, 2019.
76. Obase, T., A. Abe-Ouchi, F. Saito: Abrupt climate changes in the last two deglaciations simulated with different Northern ice sheet discharge and insolation, Scientific Reports, 11, doi: 10.1038/s41598-021-01651-2, 2021
77. Parrenin, F., Masson-Delmotte, V., Köhler, P., Raynaud, D., Paillard, D., Schwander, J., Barbante, C., Landais, A., Wegner, A., Jouzel, J.: Atmospheric carbon dioxide, methane, deuterium, and calculated Antarctic temperature of EPICA Dome C ice core. PANGAEA, doi:10.1594/PANGAEA.810199, 2013
78. Pedro, J. B., Martin, T., Steig, E. J., Jochum, M., Park, W., & Rasmussen, S. O.: Southern Ocean deep convection as a driver of Antarctic warming events. Geophysical Research Letters, 43(5), 2192–2199. https://doi.org/10.1002/2016GL067861, 2016
79. Pedro, J. B., Jochum, M., Buizert, C., He, F., Barker, S., & Rasmussen, S. O.: Beyond the bipolar seesaw: Toward a process understanding of interhemispheric coupling. Quaternary Science Reviews, 192, 27–46. https://doi.org/10.1016/j.quascirev.2018.05.005, 2018

80. Peltier, W. R., Argus, D. F., and Drummond, R.: Space geodesy constrains ice age terminal deglaciation: The global ICE-6G_C (VM5a) model, J. Geophys. Res.-Sol. Ea., 120, 450–487, 10.1002/2014JB011176, 2015.
81. Petit, J. R., Jouzel, J., Raynaud, D., Barkov, N. I., Barnola, J.-M., Basile, I., Bender, M., Chappellaz, J., Davis, M., Delaygue, G., Delmotte, M., Kotlyakov, V. M., Legrand, M., Lipenkov, V. Y., Lorius, C., PÉpin, L., Ritz, C., Saltzman, E., and Stievenard, M.: Climate and atmospheric history of the past 420 000 years from the Vostok ice core, Antarctica, Nature, 399, 429–436, 10.1038/20859, 1999.
82. Pöppelmeier, F., Jeltsch-Thömmes, A., Lippold, J. et al. Multi-proxy constraints on Atlantic circulation dynamics since the last ice age. Nat. Geosci. 16, 349–356 (2023). https://doi.org/10.1038/s41561-023-01140-3
83. Prange, M., Jonkers, L., Merkel, U., Schulz, M. and Bakker, P: A multicentennial mode of North Atlantic climate variability throughout the Last Glacial Maximum, Science, 9, 44, https://www.science.org/doi/10.1126/sciadv.adh1106, 2023.
84. Rae, J. W. B., Burke, A., Robinson, L. F., Adkins, J. F., Chen, T., Cole, C., Greenop, R., Li, T., Littley, E. F. M., Nita, D. C., Stewart, J. A. and Taylor, B. J.: CO 2 storage and release in the deep Southern Ocean on millennial to centennial timescales, Nature, 562, 569-573, https://doi.org/10.1038/s41586-018-0614-0, 2018
85. Renssen, H., Mairesse, A., Goosse, H., Mathiot, P., Heiri, O., Roche, D. M., Nisancioglu, K. H. and Valdes, P. J.: Multiple causes of the Younger Dryas cold period. Nature Geoscience, 8(12), 946–949. https://doi.org/10.1038/ngeo2557, 2015
86. Roberts, N. L., Piotrowski, A. M., McManus, J. F., and Keigwin, L. D.: Synchronous Deglacial Overturning and Water Mass Source Changes, Science, 327, 75–78, 10.1126/science.1178068, 2010.
87. Roche, D. M., Renssen, H., Paillard, D., & Levavasseur, G.: Deciphering the spatio-temporal complexity of climate change of the last deglaciation: A model analysis. Climate of the Past, 7(2), 591–602. https://doi.org/10.5194/cp-7-591-2011, 2011
88. Roche, D.M., Wiersma, A.P. & Renssen, H. A systematic study of the impact of freshwater pulses with respect to different geographical locations. Clim Dyn 34, 997–1013. https://doi.org/10.1007/s00382-009-0578-8, 2010.

89. Rojas, M., Moreno, P., Kageyama, M., Crucifix, M., Hewitt, C., Abe-Ouchi, A., Ohgaito, R., Brady E. C. andHope, P.: The Southern Westerlies during the last glacial maximum in PMIP2 simulations. Climate Dynamics, 32(4), 525–548. https://doi.org/10.1007/s00382-008-0421-7, 2009
90. Sadatzki, H., Opdyke, B., Menviel, L., Leventer, A., Hope, J. M., Brocks, J. J., Fallon, S., Post, A. L., O'brien, P. E., Grant, K., & Armand, L.: Early sea ice decline off East Antarctica at the last glacial-interglacial climate transition, Science Advances, 9, 41, doi: 10.1126/sciadv.adh9513, 2023.
91. Schloesser, F., Friedrich, T., Timmermann, A., DeConto, R. M., and Pollard, D.: Antarctic iceberg impacts on future Southern Hemisphere climate, Nat. Clim. Change, 9, 672–677, https://doi.org/10.1038/s41558-019-0546-1, 2019.
92. Seroussi, H., Nowicki, S., Payne, A. J., Goelzer, H., Lipscomb, W. H., Abe-Ouchi, A., Agosta, C., Albrecht, T., Asay-Davis, X., Barthel, A., Calov, R., Cullather, R., Dumas, C., Galton-Fenzi, B. K., Gladstone, R., Golledge, N. R., Gregory, J. M., Greve, R., Hattermann, T., Hoffman, M. J., Humbert, A., Huybrechts, P., Jourdain, N. C., Kleiner, T., Larour, E., Leguy, G. R., Lowry, D. P., Little, C. M., Morlighem, M., Pattyn, F., Pelle, T., Price, S. F., Quiquet, A., Reese, R., Schlegel, N.-J., Shepherd, A., Simon, E., Smith, R. S., Straneo, F., Sun, S., Trusel, L. D., Van Breedam, J., van de Wal, R. S. W., Winkelmann, R., Zhao, C., Zhang, T., and Zwinger, T.: ISMIP6 Antarctica: a multi-model ensemble of the Antarctic ice sheet evolution over the 21st century, The Cryosphere, 14, 3033–3070, https://doi.org/10.5194/tc-14-3033-2020, 2020.
93. Severinghaus, J. P. and Brook, E. J.: Abrupt Climate Change at the End of the Last Glacial Period Inferred from Trapped Air in Polar Ice, Science, 286, 930–934, 10.1126/science.286.5441.930, 1999.
94. Shakun, J. D., Clark, P. U., He, F., Marcott, S. A., Mix, A. C., Liu, Z., Otto-Bliesner, B., Schmittner, A., and Bard, E.: Global warming preceded by increasing carbon dioxide concentrations during the last deglaciation, Nature, 484, 49–54, 10.1038/nature10915, 2012.
95. Sherriff-Tadano, S., Abe-Ouchi, A., Yoshimori, M., Ohgaito, R., Vadsaria, T., Chan, W-L., Hotta, H., Kikuchi, M., Kodama, T., Oka, A., Southern Ocean surface temperatures and cloud biases in climate models connected to the representation of glacial deep ocean circulation, Journal of Climate. 3849-3866, https://doi.org/10.1175/JCLI-D-22-0221.1, 2023

96. Sigman, D. M., Hain, M. P., & Haug, G. H.: The polar ocean and glacial cycles in atmospheric CO2 concentration. Nature, 466(7302), 47–55. https://doi.org/10.1038/nature09149, 2010
97. Sikes, E. L., Schiraldi, B., & Williams, A.: Seasonal and Latitudinal Response of New Zealand Sea Surface Temperature to Warming Climate Since the Last Glaciation: Comparing Alkenones to Mg/Ca Foraminiferal Reconstructions. Paleoceanography and Paleoclimatology, 34(11), 1816–1832. https://doi.org/10.1029/2019PA003649, 2019.
98. Sime, L. C., Kohfeld, K. E., Le, C., Wolff, E. W., Boer, A. M. De, Graham, R. M., & Bopp, L.: Southern Hemisphere westerly wind changes during the Last Glacial Maximum: model-data comparison. Quarternary Science Reviews, 64, 104–120. https://doi.org/10.1016/j.quascirev.2012.12.008, 2013.
99. Skinner, L. C., Fallon, S., Waelbroeck, C., Michel, E., & Barker, S.: Ventilation of the deep Southern Ocean and deglacial CO2 rise. Science, 328(5982), 1147–1151. https://doi.org/10.1126/science.1183627, 2010
100. Snoll, B., Ivanovic, R.F., Valdes, P.J., Maycock, A. C. and Gregoire, L. J.: Effect of orographic gravity wave drag on Northern Hemisphere climate in transient simulations of the last deglaciation. Clim Dyn 59, 2067–2079. https://doi.org/10.1007/s00382-022-06196-2, 2022.
101. Snoll, B., Ivanovic, R., Gregoire, L., Sherriff-Tadano, S., Menviel, L., Obase, T., Abe-Ouchi, A., Bouttes, N., He, C., He, F., Kapsch, M., Mikolajewicz, U., Muglia, J., and Valdes, P.: A multi-model assessment of the early last deglaciation (PMIP4 LDv1): a meltwater perspective, Clim. Past, 20, 789–815, https://doi.org/10.5194/cp-20-789-2024, 2024.
102. Steffensen, J. P., Andersen, K. K., Bigler, M., Clausen, H. B., Dahl-Jensen, D., Fischer, H., Goto-Azuma, K., Hansson, M., Johnsen, S. J., Jouzel, J., Masson-Delmotte, V., Popp, T., Rasmussen, S. O., Röthlisberger, R., Ruth, U., Stauffer, B., Siggaard-Andersen, M.-L., Sveinbjörnsdóttir, Á. E., Svensson, A., and White, J. W. C.: High-Resolution Greenland Ice Core Data Show Abrupt Climate Change Happens in Few Years, Science, 321, 680–684, 10.1126/science.1157707, 2008.
103. Stein, K., Timmermann, A., Young Kwon, E., and Friedrich, T.: Timing and magnitude of Southern Ocean sea ice/carbon cycle feedbacks, P. Natl. Acad. Sci. USA, 117, 9, https://doi.org/10.1073/pnas.1908670117, 2020.

104. Stocker, T. F., & Johnsen, S. J.: A minimum thermodynamic model for the bipolar seesaw. Paleoceanography, 18(4), 1–9. https://doi.org/10.1029/2003PA000920, 2003
105. Stouffer, R. J., Yin, J., Gregory, J. M., Dixon, K. W., & Spelman, M. J.: Investigating the Causes of the Response of the Thermohaline Circulation to Past and. Journal of Climate, 19, 1365–1387. https://doi.org/10.1002/9781119115397.ch25, 2006
106. Tarasov, L., Dyke, A. S., Neal, R. M., and Peltier, W. R.: A data-calibrated distribution of deglacial chronologies for the North American ice complex from glaciological modeling, Earth Planet. Sci. Lett., 315–316, 30–40, 10.1016/j.epsl.2011.09.010, 2012
107. Tierney, J. E., Zhu, J., King, J., Malevich, S. B., Hakim, G. J., & Poulsen, C. J.: Glacial cooling and climate sensitivity revisited. Nature, 584(7822), 569–573. https://doi.org/10.1038/s41586-020-2617-x, 2020
108. Timmermann, A., Timm, O., Stott, L., and Menviel, L.: The roles of CO2 and orbital forcing in driving Southern Hemispheric temperature variations during the last 21 000 Yr. Journal of Climate, 22(7), 1626–1640. https://doi.org/10.1175/2008JCLI2161.1, 2009
109. Toucanne, S., Zaragosi, S., Bourillet, J.-F., Marieu, V., Cremer, M., Kageyama, M., Van Vliet-Lanoë, B., Eynaud, F., Turon, J.-L., and Gibbard, P.-L.: The first estimation of Fleuve Manche palaeoriver discharge during the last deglaciation: Evidence for Fennoscandian ice sheet meltwater flow in the English Channel ca 20–18 ka ago, Earth Planet. Sc. Lett., 290, 459–473, 2010.
110. WAIS Divide Project Members: Onset of deglacial warming in West Antarctica driven by local orbital forcing. Nature, 500(7463), 440–444. https://doi.org/10.1038/nature12376, 2013.
111. WAIS Divide project members: Precise interpolar phasing of abrupt climate change during the last ice age. Nature, 520(7549), 661–665. https://doi.org/10.1038/nature14401, 2015
112. Weitzel, N., Andres, H., Baudouin, J.-P., Kapsch, M.-L., Mikolajewicz, U., Jonkers, L., Bothe, O., Ziegler, E., Kleinen, T., Paul, A., and Rehfeld, K.: Towards spatio-temporal comparison of simulated and reconstructed sea surface temperatures for the last deglaciation, Clim. Past, 20, 865–890, https://doi.org/10.5194/cp-20-865-2024, 2024.

113. Yoshimori, M., Yokohata, T., and Abe-Ouchi, A.: A Comparison of Climate Feedback Strength between CO2 Doubling and LGM Experiments, J. Climate, 22, 3374–3395, https://doi.org/10.1175/2009JCLI2801.1, 2009.
114. Zhu, J. and Poulsen, C. J.: Last Glacial Maximum (LGM) climate forcing and ocean dynamical feedback and their implications for estimating climate sensitivity, Clim. Past, 17, 253–267, https://doi.org/10.5194/cp-17-253-2021, 2021.